

Modeling Strangeness Enhancements to resolve the Muon Excess in Cosmic Ray Extensive Air Shower Data

Julien Manshanden, Günter Sigl and Maria V. Garzelli

II. Institut für Theoretische Physik, Universität Hamburg,
Luruper Chaussee 149, 22761 Hamburg, Germany

E-mail: julien.manshanden@desy.de, guenter.sigl@desy.de,
maria.vittoria.garzelli@desy.de

Abstract. Experimental observations of extensive air showers have revealed an excess of the muon content with respect to their theoretical simulations, which we refer to as the muon puzzle. This muon puzzle hampers a precise determination of the ultra-high-energy cosmic ray mass composition. We investigate the potential of producing states of dense quark-gluon matter (which we call fireballs) to resolve the muon puzzle as quantified with data from the Pierre Auger Observatory on the depth of the shower maximum and the number of muons at ground. Adopting a phenomenological fireball model, we find that the inelasticity enhancement associated with the formation of a plasma state is in tension with data on the electromagnetic longitudinal shower development. Instead, we restrict the fireball model to only enhance the strangeness produced in Standard Model hadronic interactions, and dub this model the strangeball model. With an analytic approach based on the Heitler-Matthews model we then find explicit sets of strangeball parameters that resolve the muon puzzle. Constraints from data on shower-to-shower fluctuations of the muon number require strangeness enhancements already at energies accessible to current-generation collider experiments. At Tevatron and LHC energies we estimate 40% of the interactions to produce strangeballs, corresponding to a 5 – 9% increase of the average fraction of energy retained in the hadronic cascade compared to predictions from current hadronic interaction models. A comparison with relevant measurements of the LHCf and LHCb detectors does not directly exclude this scenario, though the obtained tension with LHCb suggests a stringent test at 14 TeV.

Keywords: Ultra-High-Energy Cosmic Rays, Pierre Auger Observatory, Muon Puzzle, Hadronic Interactions, Fireball

ArXiv ePrint: [2208.04266](https://arxiv.org/abs/2208.04266)

Contents

1	Introduction	1
2	The Fireball Model	2
3	The Impact of Fireballs on Air Shower Observables	4
3.1	Method	4
3.2	Results	4
4	A ‘Strangeball’ Extension to the Heitler-Matthews Model	8
4.1	Derivation	8
4.2	Parameter Estimation	10
4.3	Mass Dependence	12
5	Application to Auger Data	13
6	Implications for LHC measurements	16
6.1	LHCf	18
6.2	LHCb	18
7	Conclusions	20
A	Relative Muon Fluctuations	26
A.1	Modeling Relative Muon Fluctuations	27

1 Introduction

Cosmic rays (CRs) have been measured to attain energies exceeding 10^{20} eV [1]. These energies are indicative of the extreme environments responsible for their acceleration. Gaining an understanding of the CR origin is complicated by the non-trivial propagation to Earth, with the charged nature of CRs playing a prominent role. Precise measurements of the CR mass composition should provide stringent tests for current astrophysical scenarios. Due to the rapidly decreasing CR flux, the masses of CRs with energies above 10^{15} eV cannot be measured directly and must instead be inferred from the induced air showers, which leave characteristic imprints in the atmosphere and on the ground.

Some of these imprints are sensitive to the CR mass. In particular, the depth at which the shower reaches its maximum X_{\max} is a traditional mass indicator (e.g., [2, 3]). A consistent picture among further independent mass indicators could enhance the credibility and accuracy of the inferred composition (e.g., [4, 5]). Instead, various experiments found that the number of muons reaching the ground points towards a significantly heavier composition, or inversely, that current air shower simulations underestimate muon production [6–8]. This is known as the muon puzzle and can be traced back to an incomplete understanding of the hadronic interactions in air showers. Therefore, the muon puzzle also constitutes an opportunity for cosmic ray experiments to provide predictions for collider experiments regarding potentially new physics.

With ad-hoc adjustments to hadronic interaction parameters, the number of muons was found [9] to mainly depend on the total multiplicity and the fraction of all pions that are neutral. Considering also the impact of these adjustments on X_{\max} , it was shown [10] that an appropriate suppression of the fraction of energy going into electromagnetic (EM) particles has the potential to resolve the muon puzzle. Most recently this was also shown to be the case [11] when considering a phenomenological procedure of swapping pions and kaons.

Here¹ we adopt a similar procedure to investigate whether producing fireballs [13] — one of the various models proposed in the literature [10, 13–17] — in the first few interactions of an air shower could equally solve the muon puzzle. We subsequently attempt to interpret data from the Pierre Auger Observatory [18] in terms of macroscopic hadronic interaction properties by extending the analytic formalism known as the Heitler-Matthews model [19–21]. Finally, we compare our results to measurements from the LHCf and LHCb detectors at the Large Hadron Collider (LHC) and suggest some follow-up research to drive this synergy between cosmic ray and collider experiments.

This paper is structured as follows. In sections 2 and 3 we describe the fireball model and study its impact on the relevant air shower observables, respectively. The extension to the Heitler-Matthews model is outlined in section 4, and subsequently applied to Auger data in section 5. We discuss some implications of these results for measurements at the LHC in section 6, and draw our conclusions in section 7.

2 The Fireball Model

A fireball state of matter is hypothesized [13] to form when the energy density in a collision exceeds some threshold value, estimated as $1 \text{ GeV}/\text{fm}^3$. Upon formation, the fireball is a plasma consisting of deconfined up and down quarks and gluons maintained in both kinetic and chemical equilibrium. An associated high baryochemical potential leads to the fragmentation of gluons into strange quarks, resulting in an enhanced production of strange secondaries upon hadronization. This indirectly suppresses the neutral pion production compared to the Standard Model case, altering the air shower evolution [13].

In the present study we do not further develop this microscopic treatment, nor trace its connection to thermodynamical descriptions of the quark-gluon plasma (QGP) [22–28]. While the details regarding such a connection can be found in ref. [13], we proceed here with a phenomenological approach, only considering an effective enhancement of the strange particle content and an altered multiplicity and elasticity associated with fireball interactions. We note, however, that strangeness enhancements are in fact observed in heavy-ion collisions [29–32] and more recently, with ALICE at the LHC also in proton-lead [33, 34] and proton-proton collisions [35]. In contrast to a previous study, considering the production of QGPs only in the first interaction of an air shower [36], the ALICE observations open up the possibility of copious production of such quark-matter states – perhaps this fireball – in air showers and thereby potentially contribute to a solution to the muon puzzle [7, 10].

In the following we take our reference frame to be that of the Earth, with the atmospheric particles at rest providing the fixed target for the energetic air shower projectiles. These projectiles consist of the primary CRs and the produced secondaries.

The fireball state was proposed to be modeled [37] from Standard Model interactions in two steps. The enhanced multiplicity and inelasticity associated with a plasma state can be mimicked by repeated *in situ* collisions of the projectile (and its secondaries) with air nuclei

¹A more extensive description of the studies of sections 3 - 5 can be found in ref. [12].

until a specific condition is satisfied. We take this condition to be that secondary nucleons or nuclear fragments only participate in this process if their energy E_{frag} is above a fixed fraction f_{thres} of the energy of the projectile E_{proj} that initiates the fireball²:

$$E_{\text{frag}} > f_{\text{thres}} \cdot E_{\text{proj}} . \quad (2.1)$$

The enhanced production of strange particles and the associated suppression of the neutral pion production is then mimicked by swapping all pions and kaons while conserving energy, direction of momentum, and charge (with an equal probability of changing a π^0 into a K_L^0 or a K_S^0).

For this phenomenological model it is further necessary to define the condition of producing a fireball. For a fixed projectile energy, an energy-density threshold as stated above translates to a fireball-production probability due to variations of the impact parameter. We expect this probability $p(E)$ to grow with the projectile energy, as more peripheral collisions can potentially attain the fireball state. This is closely related to the core-corona picture, which was successfully applied in interpreting the centrality dependence of various observables in heavy-ion collisions [38–41]. The central region of an interaction, the core, produces a new quark matter state (similar to our fireball), while the outer region, the corona, produces particles through standard string fragmentation. From geometrical considerations and in agreement with these measurements the contribution of the core was found to increase with centrality, see, e.g., figure 4 of ref. [41]. Given the black disk limit of protons [42], a similar increase up to unity would then be expected with rising center of mass energy. Whereas in the core-corona model one typically has a superposition of both kinds of interactions in one event, the fireball is only produced with a certain probability in a given interaction.

We parametrize this fireball-production probability as follows:

$$p(E) = \begin{cases} 0 , & \text{if } E < E_{\text{min}} , \\ \left(\frac{\log(E/E_{\text{min}})}{\log(E_{\text{max}}/E_{\text{min}})} \right)^n , & \text{if } E_{\text{min}} < E < E_{\text{max}} , \\ 1 , & \text{if } E > E_{\text{max}} . \end{cases} \quad (2.2)$$

In this way no fireballs are produced below some minimum energy E_{min} . Then the production probability grows logarithmically (for $n = 1$) up to some maximum energy E_{max} , above which every interaction produces a fireball state. The approximation of having a logarithmic growth is in line with related previous works, see refs. [10, 15].

Note that swapping all pions and kaons effectively dictates the size of the strangeness enhancement in fireball interactions. This corresponds to the first approximation of ref. [37], and should also be regarded as such in this study. More flexibility could be incorporated by swapping a variable fraction of the pions and kaons. However, in the following analysis this is degenerate with the probability of eq. 2.2, and thus would not alter our results. The power n could absorb a potential energy dependence of the size of the strangeness enhancement from a single fireball, though a detailed assessment of this size is beyond the scope of this paper.

To summarize, our implementation of the fireball model has four parameters: one (f_{thres}) controlling the plasma state, and three (E_{min} , E_{max} , n) regulating the fireball-production probability.

²Under the simplification of only nuclear secondaries, our f_{thres} -parameter introduces a minimum multiplicity for fireball interactions: $n_{\text{mult}} \geq 1/f_{\text{thres}}$, with an equality symbol when equally distributing energy between the secondaries.

3 The Impact of Fireballs on Air Shower Observables

3.1 Method

To study the effect of the fireball model on the development of air showers we implemented our phenomenological model into the CONEX (version 7.5) [43, 44] module [45, 46] of CORSIKA (version 7.74) [47]. This implementation constituted altering the CNEXUS subroutine, which functions as the interface between the shower evolution and the hadronic interaction models. We compute the longitudinal (one-dimensional) shower evolution with the CASCADE TTT and AUGERHIT options, and extract X_{\max} and the number of muons N_{μ} at an altitude of 1425 m. We further set the muon detection threshold to 0.3 GeV and the shower inclination to $\theta = 67^\circ$ in accordance with the Pierre Auger Observatory study of inclined showers [48]. With this set-up the first part of the shower is computed with a Monte Carlo simulation, enabling us to also study shower-to-shower fluctuations.

We consider data from the Pierre Auger Observatory (hereafter just ‘Auger data’) on the average $\langle \cdot \rangle$ and fluctuations $\sigma(\cdot)$ of X_{\max} and $R_{\mu} = N_{\mu}/1.455 \cdot 10^7$ (for $\theta = 67^\circ$) as presented at the International Cosmic Ray Conference (ICRC) in 2019 [49]. At this stage we want to investigate whether there are fireball settings with which we can obtain a consistent interpretation of the data in terms of the CR mass composition. To do so, we explore the fireball parameter space by first fixing $f_{\text{thres}} = 0.01$ (invoking a plasma) and $E_{\min} = 10^{15}$ eV ($\Leftrightarrow \sqrt{s_{\min}} \approx 1.4$ TeV), and then we sample $E_{\max} \in \{10^{17}, 10^{18}, 10^{19}, 10^{20}\}$ eV and $n \in \{1, 2, 4, 8, 1000\}$. Note that with $n = 1000$, $p(E)$ represents a step function at E_{\max} .

For each of these fireball settings we simulate 2100 showers from proton, helium, nitrogen, silicon and iron CR primaries at an energy of 10 EeV. In this section we do not consider further energies and thus focus on the corresponding data points at this energy. Regarding the hadronic interaction models, we use QGSJETII-04 [50, 51], EPOS-LHC [52], and SIBYLL-2.3D [53] at high energies, and URQMD [54, 55] at low energies.

3.2 Results

The minimum and maximum values of the observables $\langle X_{\max} \rangle$, $\sigma(X_{\max})$, $\langle R_{\mu} \rangle$, and $\sigma(R_{\mu})/\langle R_{\mu} \rangle$ under variations of the mass composition are shown in figure 1, with the fireball settings varied along the x -axis. For the average observables these extremes simply correspond to the proton and iron predictions, but, in case of fluctuations, a mixed composition may lead to even larger values. Note that the left-most setting ($E_{\max} = 10^{20}$ eV and $n = 1000$) introduces fireballs above the energy of the primary CR and thus corresponds to the Standard Model. Accordingly, comparisons with the left-most points reveal the impact of the fireball model on the air shower observables.

For some settings the fireball model sufficiently increases $\langle R_{\mu} \rangle$ such that the extremes encompass the Auger data point (horizontal line). Simultaneously, the difference between these extremes decreases as fireballs become more abundant at lower energies. This is a universal feature of models invoking a mass-independent increase of the muon number, ultimately making the muon number less sensitive to the mass composition.

This implementation of the fireball model also affects the other observables. The reduction of $\langle X_{\max} \rangle$ can be attributed to the production of a plasma and the associated enhanced inelasticity, accelerating the shower development. This effect seems to saturate as most energy is deposited in the EM component in the first few interactions. The relative muon fluctuations are determined by the first interaction [56, 57] and are slightly enhanced for

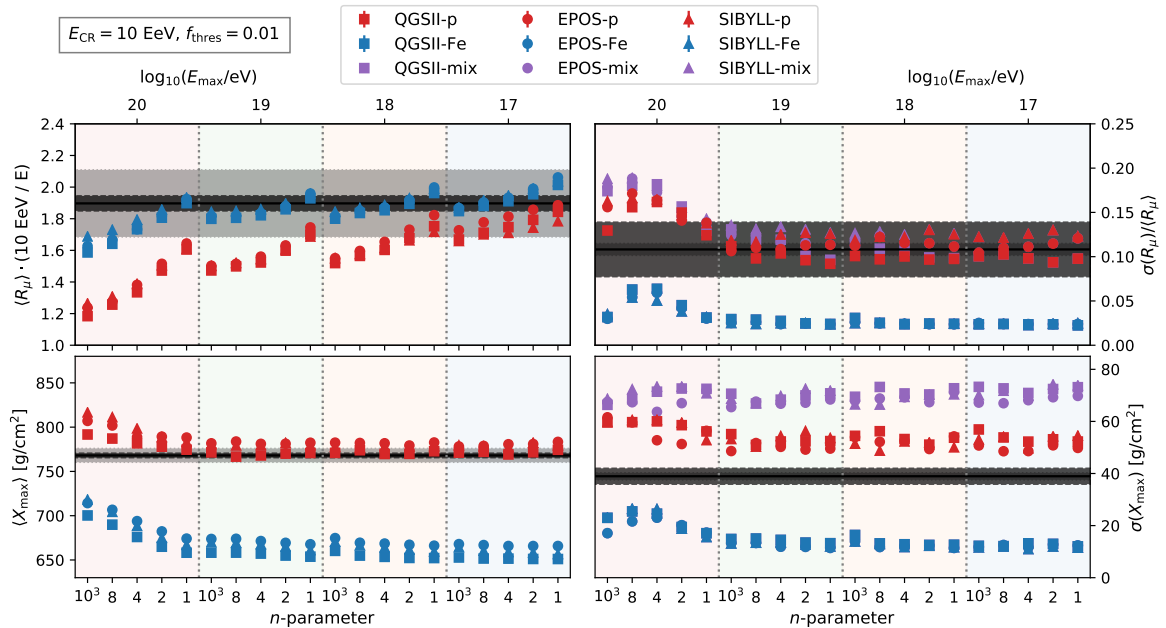


Figure 1. Impact of various settings of the fireball model on the ranges of $\langle R_\mu \rangle$ (top-left), $\sigma(R_\mu)/\langle R_\mu \rangle$ (top-right), $\langle X_{\text{max}} \rangle$ (bottom-left) and $\sigma(X_{\text{max}})$ (bottom-right) predictions from 10 EeV air showers. Varied on the x -axis are E_{max} (top axis) and n (bottom axis), while $E_{\text{min}} = 10^{15}$ eV and $f_{\text{thres}} = 0.01$ are fixed. Showers are simulated using the high-energy hadronic interaction models QGSJETII-04 (squares), EPOS-LHC (circles), and SIBYLL-2.3D (triangles) in combination with a pure proton (red) and pure iron (blue) composition. Further simulating helium, nitrogen and silicon showers enabled the computation of the mixed compositions that maximize the fluctuations (purple). Data (black horizontal lines) with systematic (light gray bands) and statistical (dark gray bands) uncertainties are from the Pierre Auger Observatory as presented at the ICRC 2019 [49].

$E_{\text{max}} = 10^{20}$ eV, $2 \leq n \leq 8$ due to a mixture of fireball and Standard Model first interactions. With only fireballs as first interactions, $\sigma(R_\mu)/\langle R_\mu \rangle$ decreases and saturates at a constant value, seeming to enforce a proton-dominated composition. A similar enhancement, decrease and saturation can be seen for $\sigma(X_{\text{max}})$, most prominently from iron showers. In contrast to the muon observables, a splitting emerges between $\sigma(X_{\text{max}})$ from mixed and pure proton compositions, reflecting the more pronounced separation of the proton and iron X_{max} distributions.

Once the predictions encompass the data points, we can infer the indicated mass composition $\{f_i\}$ from, e.g., $\langle X_{\text{max}} \rangle_{\text{data}} = \sum_i f_i \langle X_{\text{max}} \rangle_i$, with i referring to the chemical elements. Instead of solving these equations explicitly, by simultaneously considering another observable, e.g., $\langle R_\mu \rangle = \sum_i f_i \langle R_\mu \rangle_i$, we can compute the range of muon numbers that correspond to the $\langle X_{\text{max}} \rangle$ data point under variations of the composition. For average observables, the extremes of this range is guaranteed to correspond to a superposition of at most two components, which can thus be readily computed.

By comparing data on different observables, this conversion method enables us to interpret the consistency of the mass composition within a specific model. In particular, we are able to convert data on $\langle X_{\text{max}} \rangle$ to $\langle R_\mu \rangle$ and $\sigma(X_{\text{max}}) = [\langle X_{\text{max}}^2 \rangle - \langle X_{\text{max}} \rangle_{\text{data}}^2]^{1/2}$, and data on $\langle R_\mu \rangle$ to $\langle X_{\text{max}} \rangle$ and $\sigma(R_\mu)/\langle R_\mu \rangle = [\langle R_\mu^2 \rangle / \langle R_\mu \rangle_{\text{data}}^2 - 1]^{1/2}$.

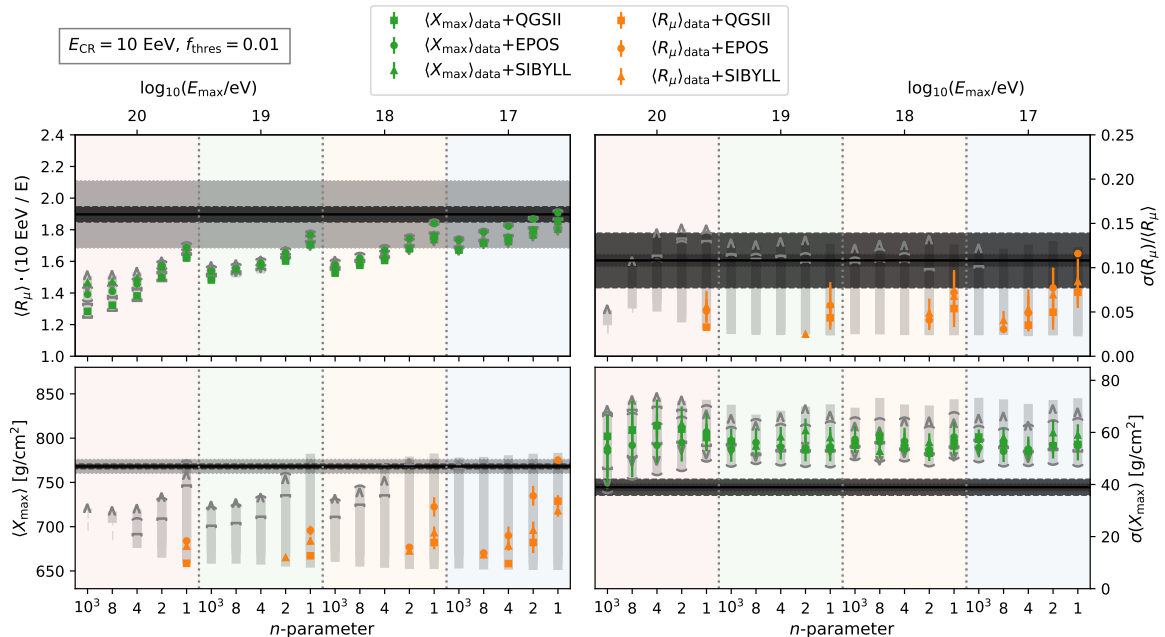


Figure 2. Similar to figure 1, but with data on $\langle X_{\max} \rangle$ and $\langle R_{\mu} \rangle$ converted to the other observables through model predictions, see text for more detail. The error bars represent the variation due to a degeneracy of the composition. The (total) uncertainties are visualized through the vertical gray bars, ending where the observable falls outside of allowed range of predictions (i.e., beyond proton, iron, extreme mix).

The application of this method to the fireball settings of figure 1 is shown in figure 2. Here it becomes clear that consistency between data on $\langle X_{\max} \rangle$ and $\langle R_{\mu} \rangle$ is found for $E_{\max} = 10^{17}$ eV and $n = 1$ with EPOS-LHC. However, the fireball model seems to introduce an inconsistency between data on $\langle X_{\max} \rangle$ and $\sigma(X_{\max})$, with the average indicating a significantly lighter composition than the fluctuations. This can be traced back to the formation of a plasma accelerating the shower development. Therefore, we repeated the analysis for other values of $f_{\text{thres}} \in \{1, 0.1, 0.001\}$. It turns out that the aforementioned inconsistency can only be avoided if one turns off the formation of a plasma by setting $f_{\text{thres}} = 1$, reducing fireball interactions to correspond to only swapping pions and kaons. The impact on the observables are shown in figure 3. Notice that these fireballs only affect the muon number (both average and fluctuations), leaving X_{\max} unaffected. For the settings summarized in table 1 we find that a solution of the muon puzzle is possible at $E_{\text{CR}} = 10$ EeV.

Table 1. Settings of the fireball model enabling a consistent composition interpretation of data from the Pierre Auger Observatory as presented at the ICRC 2019 [49], on both moments of X_{\max} and R_{μ} at 10 EeV.

	$\log_{10}(E_{\min}/\text{eV})$	$\log_{10}(E_{\max}/\text{eV})$	n	f_{thres}
QGSJETII-04	15	17	2	1.0
EPOS-LHC	15	18	1	1.0
	15	17	4	1.0
SIBYLL-2.3D	15	18	1	1.0
	15	17	4	1.0

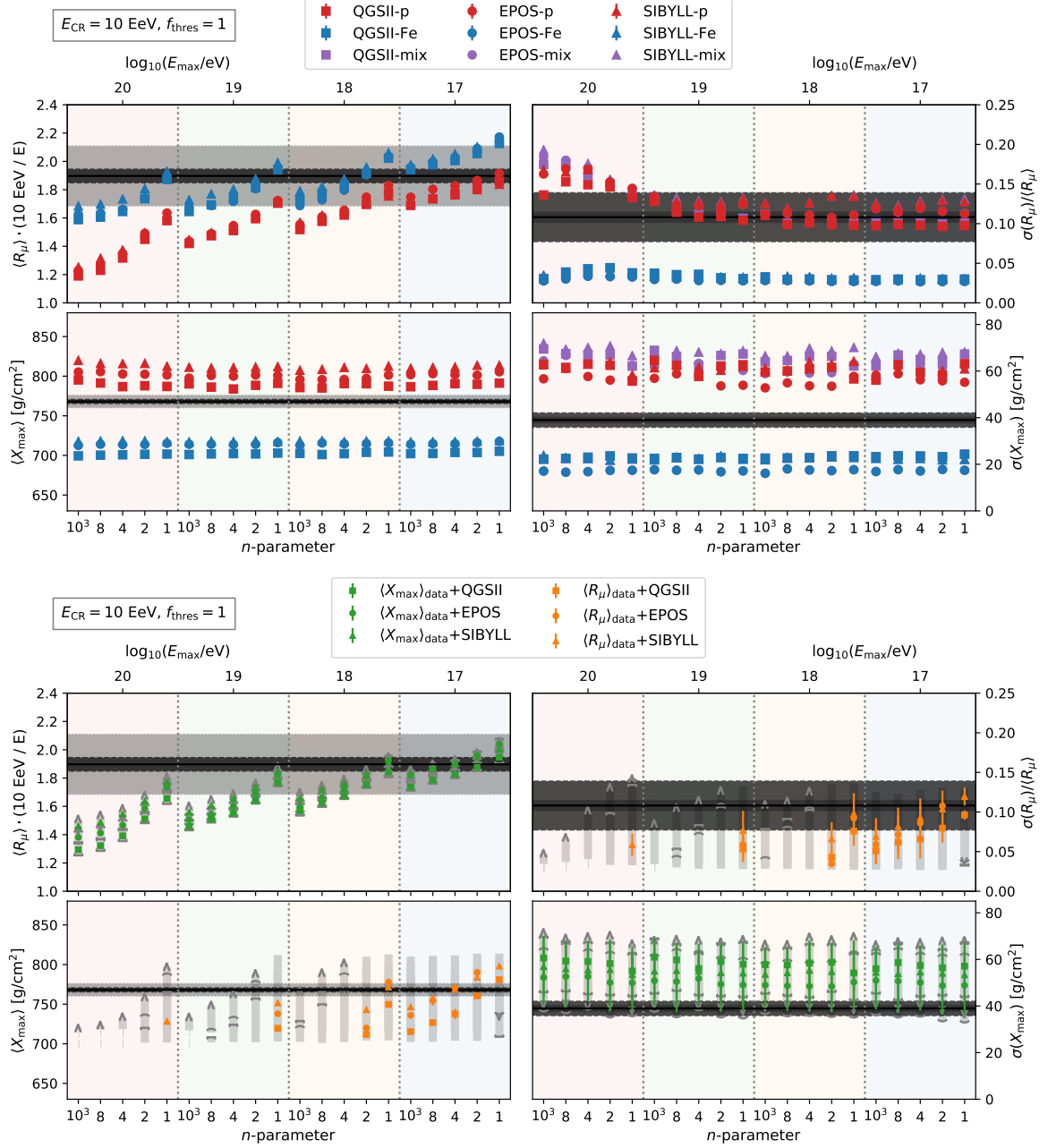


Figure 3. Same as figures 1 (top) and 2 (bottom), but then for $f_{\text{thres}} = 1$.

4 A ‘Strangeball’ Extension to the Heitler-Matthews Model

From section 3 we know that only a reduced fireball model — where no plasma is formed and the multiplicity is unaltered — could potentially resolve the muon puzzle. Without the formation of a plasma state, it may be misleading to continue calling this a “fireball”. Therefore, lacking a better word, we will refer to this reduced fireball as a “strangeball”. It is interesting to note that the rope hadronization model for string fragmentation [58–61] actually provided the best description of the ALICE strangeness enhancements in proton-proton collisions [35] without invoking the formation of a plasma. Perhaps this could provide an alternative microscopic picture for strangeball formation. For the remainder of this work we thus consider a *strangeball* model, which consists solely of an appropriate swapping of pions and kaons, and thus only affects the muon number. An extension of the previous analysis to other CR energies could then be attempted with an analytic approach, starting from the Heitler-Matthews model [19–21].

4.1 Derivation

In the Heitler-Matthews model a hadronic air shower is modeled as consisting of charged and neutral pions. Neutral pions promptly decay to two photons, leaking energy from the hadronic component to EM showers. The charged pions produce further sets of charged and neutral pions until their energies fall below the critical energy — defined as where the decay length becomes shorter than the interaction length — at which point they decay to muons in a 1:1 ratio.

The number of muons thus corresponds to the number of charged pions at the end of a shower. Assuming the production of n_{mult} pions in an interaction, of which a fraction r is charged, one has $(rn_{\text{mult}})^k$ charged pions after k interactions (or generations). With the further strong assumption of dividing the projectile energy equally over all produced pions, the critical generation k_c (where charged pions reach the critical energy E_c) follows from $E_0/n_{\text{mult}}^{k_c} = E_c$, with E_0 the energy of the CR primary. Combining these, the muon number at the end of the shower is given by

$$N_{\mu} = (rn_{\text{mult}})^{k_c} = \left(\frac{E_0}{E_c}\right)^{\beta}, \quad (4.1)$$

where $\beta \equiv \log(rn_{\text{mult}})/\log(n_{\text{mult}})$ [9].

Swapping pions and kaons mainly induces a suppression of the produced number of neutral pions. Therefore, strangeball interactions differ from the Standard Model ones by an increased fraction of energy remaining in the hadronic component after an interaction. In the Heitler-Matthews model this fraction $r \equiv E_{\text{had}}/E_{\text{proj}}$ is constant, but in our extension we allow it to vary throughout the shower, taking at projectile energy E the effective value

$$r_{\text{eff}}(E) \equiv [1 - p(E)]r_{\text{SM}} + p(E)r_{\text{sb}}, \quad (4.2)$$

where r_{SM} and r_{sb} are the values for Standard Model and strangeball interactions, respectively, and $p(E)$ is the strangeball-production probability (eq. (2.2)).

From $d \log(N_{\text{had}}/N_{\text{tot}})/dk = d \log((rn_{\text{mult}})^k/n_{\text{mult}}^k)/dk = \log r$ we see that r quantifies the generational change of the fraction of particles in the hadronic component. With an exponentiation and a multiplication by the total number of particles as fixed by the critical

energy $N_{\text{tot}} = E_0/E_c$, we can incorporate an energy-dependent r -value for the computation of the muon number:

$$N_\mu = \left(\frac{E_0}{E_c}\right) \exp \left[\int_0^{k_c} \log\{r_{\text{eff}}(E)\} dk + \Delta_{\text{disc}} \right]. \quad (4.3)$$

Here the upgrade of k from a discrete to a continuous variable required the correction term $\Delta_{\text{disc}} \equiv \frac{1}{2} \log(r_{\text{sb}}/r_{\text{SM}}) p(E_0)$, constituting an additional half generation of strangeballs. This takes into account that the type of interaction is determined by the incoming particles.

The multiplicity relates the generation k to the energy E of the particles at that generation. In the Heitler-Matthews model we have $E = E_0/n_{\text{mult}}^k$, but at this point we can also consider an energy-dependent multiplicity. Taking a power-law,

$$n_{\text{mult}}(E) = n_{\text{scale}} \left(\frac{E}{1 \text{ GeV}} \right)^b, \quad (4.4)$$

we can solve the recurrence relation $E_{k+1} = E_k/n_{\text{mult}}(E_k)$, which enables the computation of the Jacobian $dk/d \log E$ for the integral of eq. (4.3).

Using our parametrization of the fireball (i.e. strangeball) production probability (eq. (2.2)) along with eq. (4.2) and the power-law multiplicity (eq. (4.4)), we compute the muon number through eq. (4.3) as

$$N_\mu = \left(\frac{E_0}{E_c}\right) \left[\frac{x_c}{x_0}\right]^{c_1} \times \begin{cases} 1, & \text{if } E_0 \leq E_{\text{min}}, \\ \left(\frac{E_0}{E_{\text{min}}}\right)^{\delta'(E_0)}, & \text{if } E_{\text{min}} \leq E_0 \leq E_{\text{max}}, \\ \left(\frac{E_{\text{max}}}{E_{\text{min}}}\right)^{\delta'(E_{\text{max}})} \left[\frac{x_{\text{max}}}{x_0}\right]^{c_2}, & \text{if } E_0 \geq E_{\text{max}}, \end{cases} \quad (4.5)$$

where we defined

$$c_1 \equiv \frac{\log r_{\text{SM}}}{\log(1-b)}, \quad c_2 \equiv \frac{\log(r_{\text{sb}}/r_{\text{SM}})}{\log(1-b)}, \quad (4.6)$$

$$x_i \equiv \log \left(n_{\text{scale}} \left(\frac{E_i}{1 \text{ GeV}} \right)^b \right), \quad i \in \{c, 0, \text{min}, \text{max}\}, \quad (4.7)$$

$$\delta'(E) \equiv -\frac{p(E)}{n+1} \frac{c_2}{x_{\text{min}}/b} {}_2F_1 \left(1, 1+n; 2+n; \frac{-\log(E/E_{\text{min}})}{x_{\text{min}}/b} \right) + \frac{1}{2} \frac{\log(r_{\text{sb}}/r_{\text{SM}})}{\log(E_{\text{max}}/E_{\text{min}})} p(E)^{\frac{n-1}{n}}, \quad (4.8)$$

for compactness and readability. The function ${}_2F_1(a, b; c; x)$ is the hypergeometric function.

The three energy regimes of $p(E)$ is reflected here as a collection of distorted power-laws. Below E_{min} the power-law of the Heitler-Matthews model (eq. (4.1)) transforms to a power-law of logarithmic terms (eq. (4.7)) due to the energy-dependent multiplicity. The transition region from no strangeballs to only strangeballs is characterized by a further power-law with an energy-dependent slope (eq. (4.8)). Above E_{max} one again obtains the transformed power-law with logarithmic terms, but then with the slope adjusted for strangeballs (eq. (4.6)).

4.2 Parameter Estimation

Summarizing the parameters, we have the strangeball settings $\{E_{\min}, E_{\max}, n\}$ (also through $p(E)$ in eq. (4.8)), the physical quantities $\{r_{\text{SM}}, r_{\text{sb}}, n_{\text{scale}}, b, E_c\}$, and the energy E_0 of the primary CR. For the application of this framework to Auger data we need to estimate the physical quantities.

Since the hadronic energy fraction and the multiplicity are properties of individual interactions, we attempted to obtain $\{r_{\text{SM}}, r_{\text{sb}}, n_{\text{scale}}, b\}$ from the high-energy hadronic interaction models directly. We used the CRMC software package [62] as a uniform interface to QGSJETII-04, EPOS-LHC, and SIBYLL-2.3C³ [63], simulating 10^4 fixed-target collisions of energetic proton and π^+ projectiles with stationary proton and nitrogen targets, varying the projectile energy from 10^2 GeV to 10^{11} GeV in steps of factors of 10.

From each collision we computed the fraction of the projectile energy that is carried away by hadronic secondaries, counting all particles but $\{\pi^0, e^\pm, \gamma\}$ for the Standard Model, and all particles but $\{K_{L/S}^0, e^\pm, \gamma\}$ for the strangeball model. Changing the projectile energy or the type of interacting particles induce variations of $\langle r_{\text{SM}} \rangle$ ($\langle r_{\text{sb}} \rangle$) within 0.1 (0.05). In our simplified approach we ignore these variations and computed the global averages, giving equal weights to all energies and projectile-target combinations, resulting in the parameters listed in table 2. We further computed the total multiplicity of each collision, finding the averages among many collisions to follow a power-law with projectile energy, for each projectile-target combination. Averaging these power laws with equal weights (point-wise at each energy) resulted in a global power law, of which the parameters are also listed in table 2.

Table 2. Estimates of the parameters related to physical quantities for the evaluation of eq. (4.5), using both CRMC and CONEX simulations and various hadronic interaction models.

		r_{SM}	r_{sb}	n_{scale}	b	E_c [GeV]
CRMC	QGSJETII-04	0.781	0.937	5.69	0.193	-
	EPOS-LHC	0.788	0.930	7.70	0.166	-
	SIBYLL-2.3C	0.803	0.921	6.74	0.173	-
CONEX	QGSJETII-04	0.509	0.720	968	$8.68 \cdot 10^{-2}$	136
	EPOS-LHC	0.550	0.764	3820	$2.58 \cdot 10^{-3}$	154
	SIBYLL-2.3D	0.565	0.736	3230	$3.92 \cdot 10^{-5}$	151

Since we implicitly consider the hadronic shower component to consist of more than just charged pions, the definition of a single critical energy becomes ambiguous. Therefore, instead of estimating its value from first principles (through the interaction and decay lengths), we treat it as a normalization parameter. Setting it to $E_c = 220$ GeV and using the remaining parameters from CRMC, the number of muons as a function of primary energy E_0 from eq. (4.5) is given by the dashed lines of figure 4 for EPOS-LHC and $E_{\min} = 10^{15}$ eV.

We ran an additional set of CONEX simulations to evaluate the validity of this approach. Only considering proton CRs, we explored the strangeball phase-space varying $E_{\min} \in \{10^{14}, 10^{15}, 10^{16}\}$ eV, $E_{\max} \in \{10^{17}, 10^{18}, 10^{19}, 10^{20}\}$ eV, and $n \in \{1, 2, 4, 8, 1000\}$. The energy-dependence of the average muon number is sampled with $E_0 \in \{1, 2, 5, 10, 20, 50, 100,$

³At the time of this study, the updated version SIBYLL-2.3D was not yet available in CRMC.

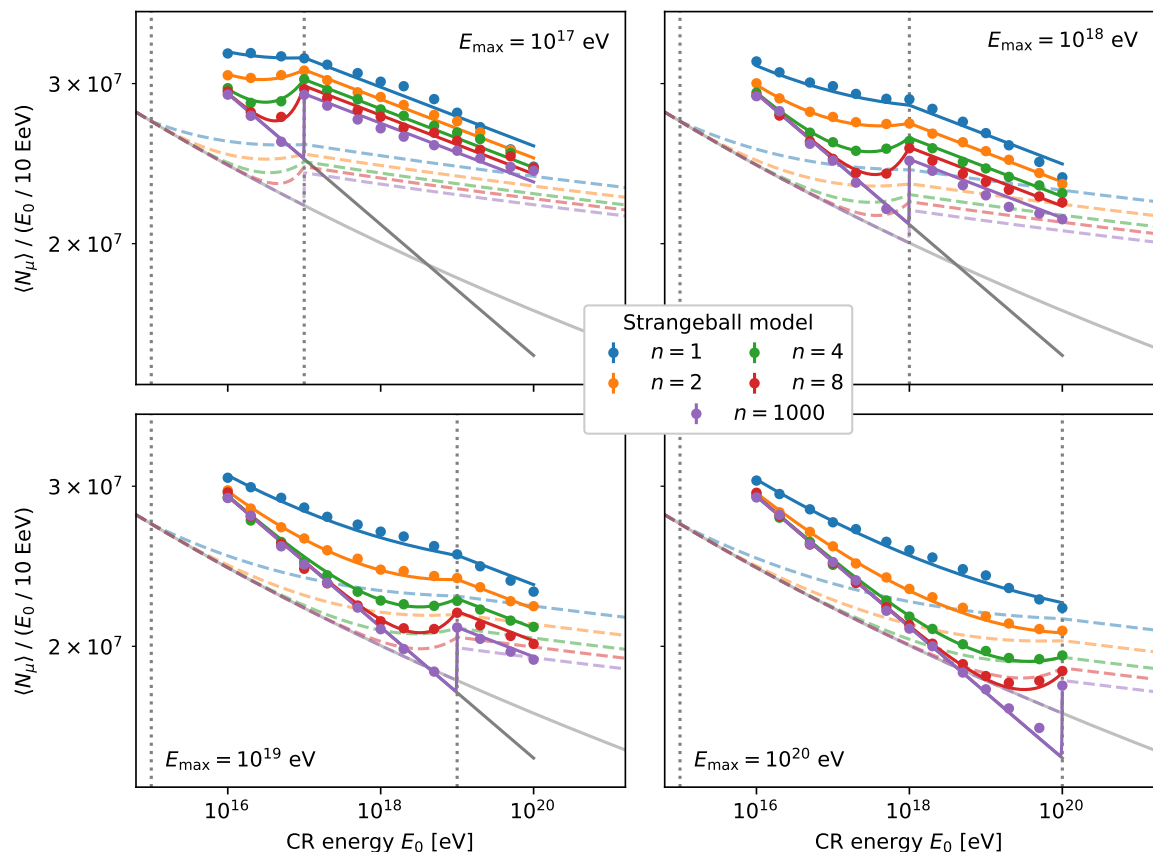


Figure 4. Energy dependence of the average muon number for various strangeball settings with EPOS-LHC as obtained with CONEX simulations (data points) fitted with eq. (4.5) (solid lines), and using CRMC-inferred parameters directly with eq. (4.5) (dashed lines). The gray lines correspond to the no strangeball case, and we fixed $E_{\min} = 10^{15}$ eV.

200, 500, 1000, 2000, 5000, 10000} $\times 10^{16}$ eV, and the simulations are repeated for the hadronic interaction models QGSJETII-04, EPOS-LHC, and SIBYLL-2.3D, simulating 2100 showers for each setting. The resulting values for EPOS-LHC and $E_{\min} = 10^{15}$ eV are indicated by the points (with negligible statistical uncertainty) in figure 4.

Independent of our choice of E_c , the muon numbers from CONEX simulations are not reproduced by eq. (4.5) when using the parameters inferred from CRMC simulations. This implies that our attempt to connect microscopic parameters to a macroscopic observable with an analytic model is too simplistic. This inadequacy can most likely be traced back to the unphysical Heitler-Matthews assumption of equally dividing the projectile energy over all secondaries, which is in direct contradiction with the CRMC spectra. One may consider combining our strangeball extension with the extension presented in [64] to take into account leading particle effects.

Instead, since the functional form given by the CONEX simulations seems to be reproduced, we fitted eq. (4.5) directly to the results of these simulations (fixing $E_{\min} = 10^{15}$ eV; 260 data points), as shown by the solid lines in figure 4. This gave a surprisingly good fit, where we obtained a single set of parameters for each model as listed in table 2. It thus seems that realistic effects such as that of leading particles can be absorbed into these parameters,

making them effective and their physical interpretation should be met with some caution. The same parameters provided a similarly good description of the CONEX simulations with $E_{\min} \in \{10^{14}, 10^{16}\}$ eV, implying that eq. (4.5) can be used to interpolate the average muon number N_μ in the primary energy E_0 , as well as the three strangeball settings E_{\min} , E_{\max} , and n .

4.3 Mass Dependence

Now we need to introduce a mass dependence to our analytic model by way of the superposition principle:

$$N_\mu(E_0, A) = A \cdot N_\mu(E_0/A, 1) . \quad (4.9)$$

This states that the muon number from a shower initiated by a CR with energy E_0 and mass A corresponds to that of A protons, each a factor A lower in energy. We assume that the total energy, rather than that per nucleon, is decisive for the production of a strangeball state. Note that in this case the conventional superposition principle underestimates the strangeball production from nuclei. This becomes especially apparent when considering a rapidly changing strangeball production probability $p(E)$, as illustrated in figure 5 (e.g., the line with $E_{\max} = 10^{19}$ eV and $n = 1$).

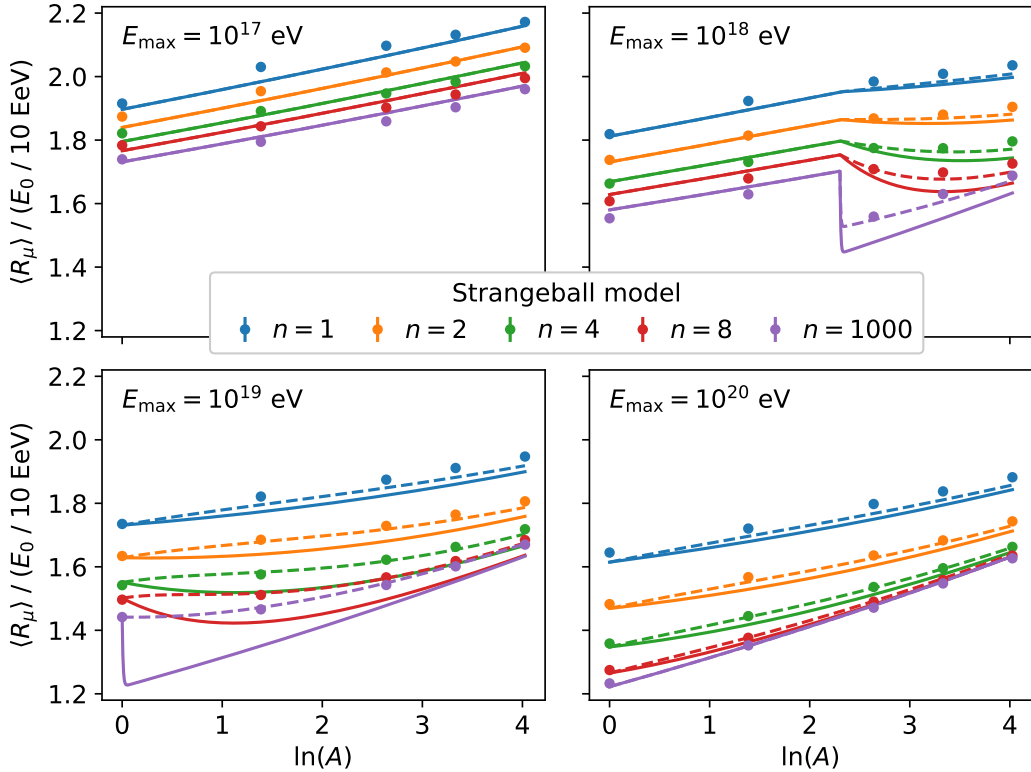


Figure 5. Mass dependence of the average muon number at 10 EeV for various strangeball settings obtained from EPOS-LHC CONEX simulations (data points) and compared with our analytic model (eq. (4.5) with CONEX parameters of table 2) by applying the superposition principle (eq. (4.9), solid lines) and when including our correction factor (with eq. (4.10), dashed lines).

We introduce a correction factor to the right-hand side of eq. (4.9),

$$u + (1 - u) \cdot [r_{\text{sb}}/r_{\text{SM}}]^{\Delta p/2} , \quad (4.10)$$

where u denotes the fraction of the nucleus that does not participate in the first inelastic interaction (‘spectator nucleons’), and is thus unaffected by the strangeball state. The remainder of the nucleus finds its muon production enhanced by half a generation of additional strangeballs, weighted by the difference in strangeball-production probability for the nucleus and its nucleons: $\Delta p \equiv p(E_0) - p(E_0/A)$. This correction factor is equivalent to revising Δ_{disc} of eq. (4.3) to be evaluated at the energy of the nucleus rather than that of its nucleons.

We found a good agreement with EPOS-LHC CONEX simulations when setting $u = 1 - 1/\sqrt{A}$, as indicated by the dashed lines in figure 5. This corresponds to approximately \sqrt{A} nucleons interacting inelastically. While a slight deviation remains for the other two models, we expect our approximation to suffice for the current study.

5 Application to Auger Data

Equipped with eq. (4.5), its parameters, and a mass dependence, we looked for strangeball settings that reproduce Auger data. First, we verified with CONEX simulations that the statistical moments of X_{max} are unaffected by the strangeball model. We simulated proton and iron showers with energy in the range from $10^{17} - 10^{20}$ eV and strangeball settings $E_{\text{min}} = 10^{15}$ eV, $E_{\text{max}} \in \{10^{17}, 10^{18}, 10^{19}, 10^{20}\}$ eV, and $n \in \{1, 2, 4, 8, 1000\}$, for each hadronic interaction model. We did not find a significant deviation with respect to simulations without strangeballs, justifying our approach to only consider changes to the muon number. This puts us in a situation where we can assume the composition from X_{max} to be the true composition and that we only need to adjust the muon predictions until they give the same picture.

By mapping data on $\langle X_{\text{max}} \rangle$ to $\langle R_{\mu} \rangle$ we can directly quantify the size of the muon discrepancy, as visualized in figure 6 for EPOS-LHC. In the top plot we find the $\langle X_{\text{max}} \rangle$ predictions to follow power-laws in energy, enabling a straightforward interpolation to the energies of the data points. The interpolation in energy of $\langle R_{\mu} \rangle$ comes from our analytic model, with which we mapped the $\langle X_{\text{max}} \rangle$ data to the bottom plots following the same procedure as in section 3. These plots correspond to opposite extremes of the strangeball settings: a gradual introduction of strangeballs starting at low energies (10^{13} eV; left), or an abrupt introduction around 10^{17} eV (right). Considering only these data, both scenarios seem to resolve the muon puzzle.

A distinction could be made by including information on the relative muon fluctuations (e.g., [65]), which reflects the physics of the first interaction. In appendix A we explored the effect of strangeballs on the energy dependence of these fluctuations following a modeling similar to that of section 4. We found that strangeballs in the first interaction tend to decrease the relative muon fluctuations, which could lead to shifting the muon puzzle to these fluctuations. This effectively puts a lower limit on E_{max} , requiring a 100% probability of producing strangeballs to be only allowed at energies above what is measured by the Pierre Auger Observatory.

For a complete exploration of the phase-space of strangeball settings we fixed $n \in \{1, 2, 4, 8, 1000\}$ and varied both $10^{12} \leq E_{\text{min}}/\text{eV} \leq 10^{18}$ and $10^{16} \leq E_{\text{max}}/\text{eV} \leq 10^{22}$. As visualized in figure 7 for EPOS-LHC (similar figures were obtained for QGSJETII-04 and SIBYLL-2.3D) we computed for each setting a chi-squared statistic to quantify the agreement

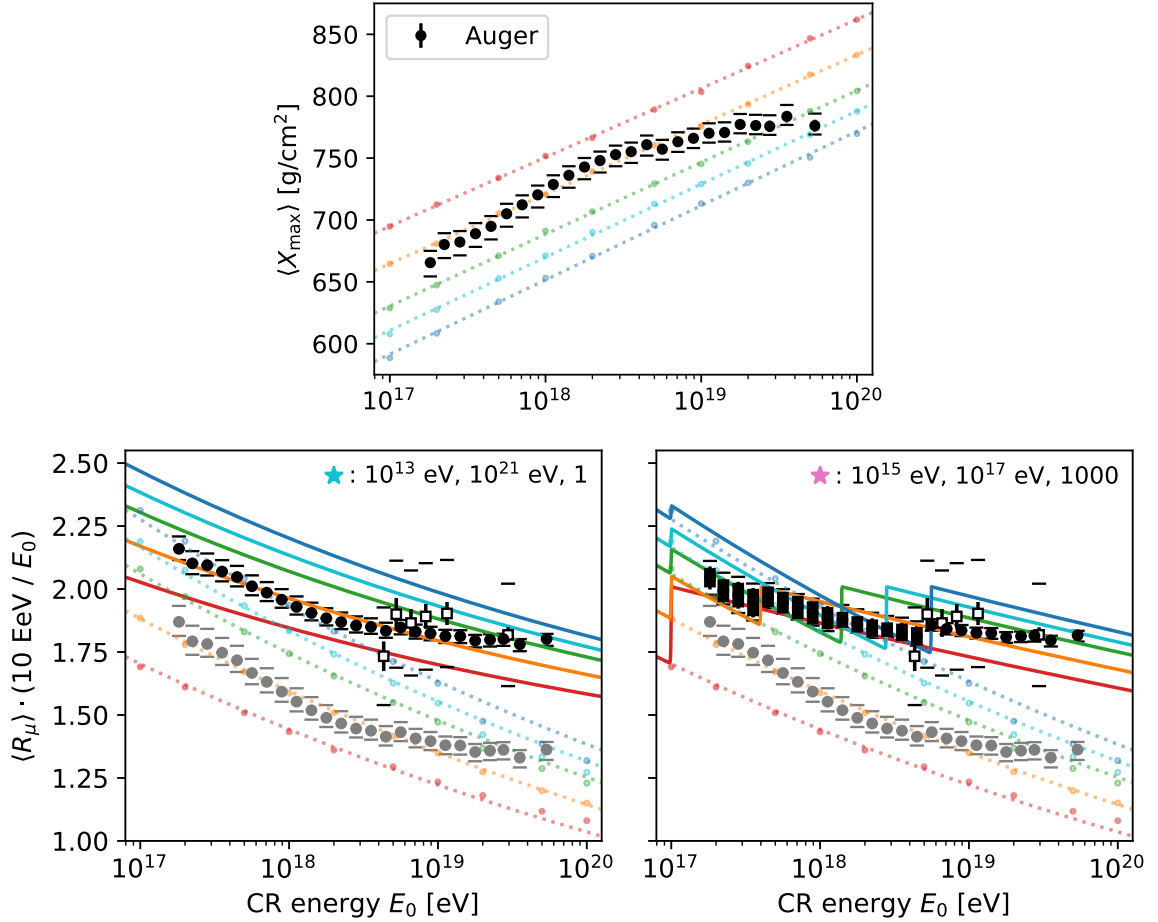


Figure 6. Composition inference from Auger data (error bars) on $\langle X_{\max} \rangle$ (top) and $\langle R_{\mu} \rangle$ (bottom) using EPOS-LHC and the strangeball model. The strangeball model (solid lines) leaves $\langle X_{\max} \rangle$ unaffected, data on which (black error bars) can thus be interpreted within the Standard Model (dotted lines). In the bottom plots a direct comparison with $\langle R_{\mu} \rangle$ data (white square error bars) follows from mapping $\langle X_{\max} \rangle$ data to $\langle R_{\mu} \rangle$ within the Standard Model (gray error bars) and the following two strangeball scenarios (black error bars): $E_{\min} = 10^{13} \text{ eV}$, $E_{\max} = 10^{21} \text{ eV}$ and $n = 1$ (bottom left), and $E_{\min} = 10^{15} \text{ eV}$, $E_{\max} = 10^{17} \text{ eV}$ and $n = 1000$ (bottom right). The line colors correspond to various nuclei: proton (red), helium (orange), nitrogen (green), silicon (cyan), and iron (blue).

between data on $\langle X_{\max} \rangle$ and $\langle R_{\mu} \rangle$:

$$\chi^2(E_{\min}, E_{\max}, n) \equiv \sum_{i=1}^6 \frac{[\langle R_{\mu} \rangle_{\langle X_{\max} \rangle \text{ data}}(E_i; E_{\min}, E_{\max}, n) - \langle R_{\mu} \rangle_{\text{data}, i}]^2}{\delta \langle R_{\mu} \rangle_{\text{syst}, i}^2 + \delta \langle R_{\mu} \rangle_{\text{stat}, i}^2}. \quad (5.1)$$

The sum runs over the six muon data points and $\langle R_{\mu} \rangle_{\langle X_{\max} \rangle \text{ data}}(E_i; E_{\min}, E_{\max}, n)$ represents the mapped data on $\langle X_{\max} \rangle$, which is subsequently linearly interpolated in $\log E$ to the energies E_i of the data points $\langle R_{\mu} \rangle_{\text{data}, i}$. We neglect the uncertainty on $\langle X_{\max} \rangle$ data and consider the total uncertainty on $\langle R_{\mu} \rangle$ data to correspond to a quadratic sum of the systematic $\delta \langle R_{\mu} \rangle_{\text{syst}, i}$ and statistical $\delta \langle R_{\mu} \rangle_{\text{stat}, i}$ uncertainties. Note that a division of $\langle R_{\mu} \rangle$ by energy is

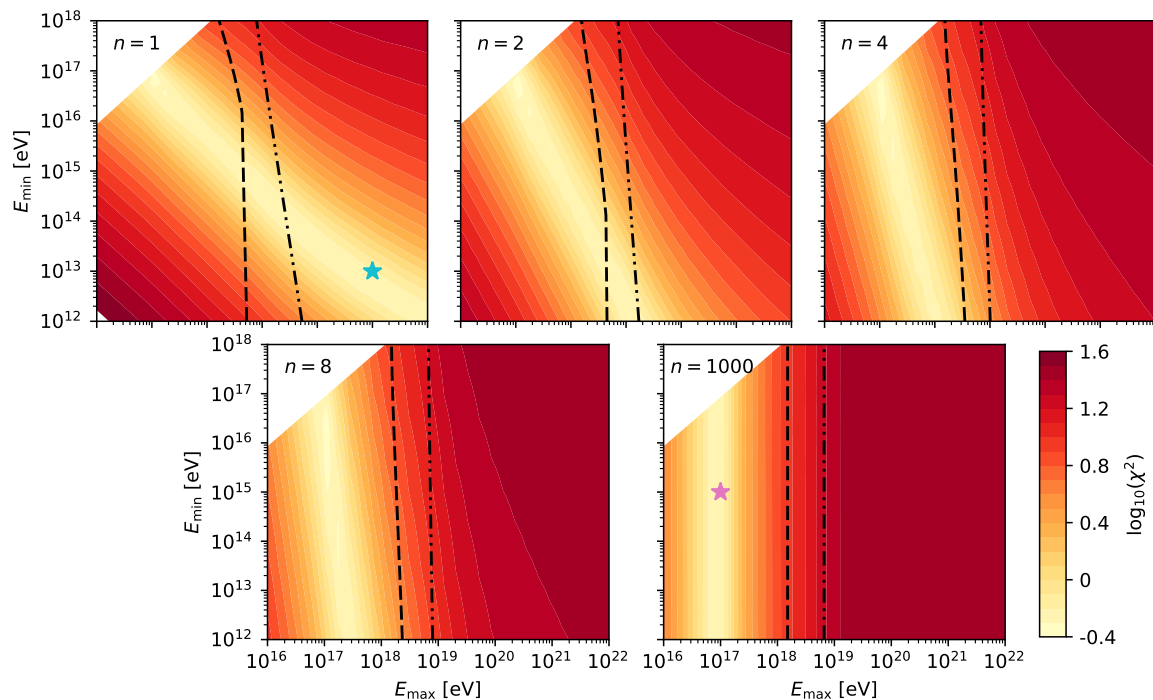


Figure 7. Strangeball parameter-space exploration of the compatibility of the composition inference of Auger data on $\langle X_{\max} \rangle$ and $\langle R_{\mu} \rangle$ as quantified by the test statistic χ^2 (eq. (5.1)) for EPOS-LHC. A lower χ^2 implies a better compatibility. The inset stars correspond to the central (cyan) and right (purple) plots in figure 6. The black lines are lower limits on E_{\max} required by data on the muon fluctuations.

canceled by the uncertainty term.

A resolution of our muon puzzle follows from enhancing the $\langle R_{\mu} \rangle$ predictions to a certain plateau, which only corresponds to a single constraint on the strangeball settings. This is reflected by the valleys of solutions in figure 7 for each value of n . Lower limits on E_{\max} from data on the relative muon fluctuations are indicated by the black lines, to the left of which proton predictions fall more than 1σ below these data (and the expected heavier composition corresponds to an even larger tension). Combining these constraints we find that with fluctuations limiting the number of strangeballs in the first interaction, strangeballs need to be present at lower energies, to reach the plateau and resolve the muon puzzle. This roughly excludes scenarios with $n > 1$, favoring the gradual (blue star) over the abrupt (purple star) solution.

Considering only $n = 1$, the combinations of E_{\min} and E_{\max} that minimize χ^2 are shown on the left of figure 8 for each hadronic interaction model. Note that E_{\max} starts at 10^{18} eV and thus already roughly takes into account the constraint from the fluctuations. The lower values for QGSJETII-04 reflects its lower muon numbers. We converted these solutions to the probability of producing strangeballs (central plot) and the effective enhancement to the hadronic energy fraction (right plot) at LHC ($\sqrt{s_{\text{LHC}}} = 13$ TeV $\Leftrightarrow E_{\text{LHC}} = 8.45 \cdot 10^{16}$ eV) and Tevatron ($\sqrt{s_{\text{Tev}}} = 2$ TeV $\Leftrightarrow E_{\text{Tev}} = 2 \cdot 10^{15}$ eV) energies. Only for the lowest allowed values of E_{\max} may strangeball effects be invisible at Tevatron energies. More compatible with the constraints from the fluctuations, we find any solution to the muon puzzle to require 35–40%

(40 – 45%) of the interactions to be strangeballs at Tevatron (LHC) energies, corresponding to an effective increase of the hadronic fraction of 5 – 8% (6 – 9%).

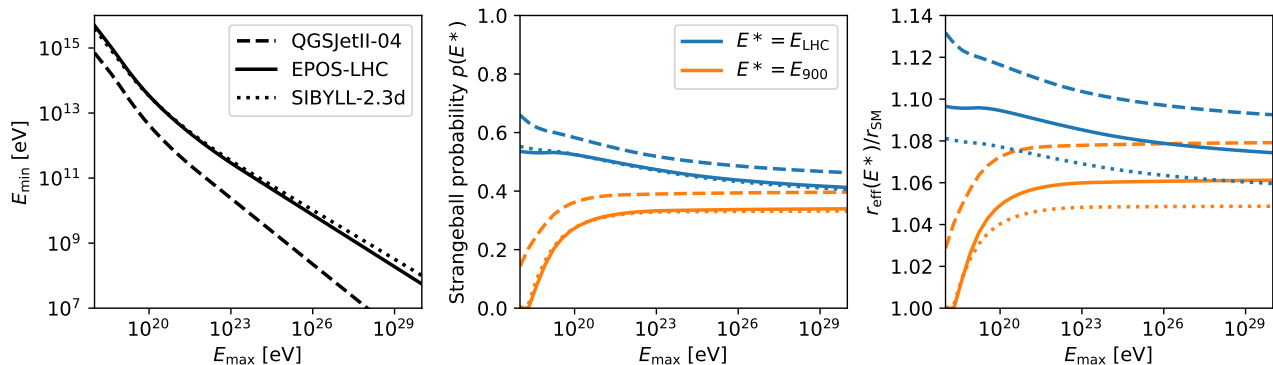


Figure 8. *Left:* Strangeball settings resolving the muon puzzle without violating constraints from the muon fluctuations (i.e., $E_{\max} \gtrsim 10^{19}$ eV). *Center and right:* Conversion of these strangeball settings to the strangeball-initiation probability (center, eq. (2.2)) and effective enhancement of the hadronic energy fraction (right, eq. (4.2)) at LHC (blue, $E_{\text{LHC}} \approx 10^{17}$ eV) and Tevatron (orange, $E_{\text{Tev}} \approx 10^{15}$ eV) energies.

Some care is needed in the interpretation of these results. Solutions to the muon puzzle in terms of E_{\min} and E_{\max} combinations and the subsequent conversion to a strangeball probability rely on the correct interpolation (and extrapolation) of our analytic model in terms of the CR energy and the strangeball settings. We verified this with CONEX simulations for a subset of settings ($10^{14} \leq E_{\min}/\text{eV} \leq 10^{16}$ and $10^{17} \leq E_{\max}/\text{eV} \leq 10^{20}$), as in, e.g., figure 4. Many of the solutions in figure 8 are outside this range, but, given the physical assumptions going into our model, we do not expect large uncertainties associated to these extrapolations. For the subsequent conversion to an effective increase of the hadronic energy fraction we employed eq. (4.2) with the parameters listed in table 2. Since the parameters inferred from CONEX simulations are likely unphysical, with in particular the very high multiplicities, we used the representative parameters found with CRMC simulations instead.

6 Implications for LHC measurements

The hadronic energy fraction r is not a directly measurable quantity at collider experiments. Therefore, it is worthwhile to translate our results to observables of the relevant detectors at the LHC. For this we need to explicitly specify the model under consideration. The analytic model of section 4 is agnostic towards the precise origin of enhancing r , which implies that the results in the right-most plot of figure 8 could be regarded as independent of the model behind the enhancement (e.g., swapping). Furthermore, a phenomenological model valid for air showers may not necessarily be valid for collider experiments. Nevertheless, for the sake of consistency and simplicity, we will stick to modeling strangeballs by swapping pions for kaons.

We would further like to point out that our focus on r represents a generic approach to resolving the muon puzzle. This follows from an assumed proportionality between the energy kept in the hadronic shower component and the produced number of muons. However, by swapping particles or otherwise adjusting the hadronic particle spectra one may also enhance the efficiency of converting hadronic energy into the production of muons. To analyze this

effect on the muon number it is convenient to reverse the problem and study their genealogy (see, e.g., refs. [66, 67]), but such considerations are beyond the scope of this paper.

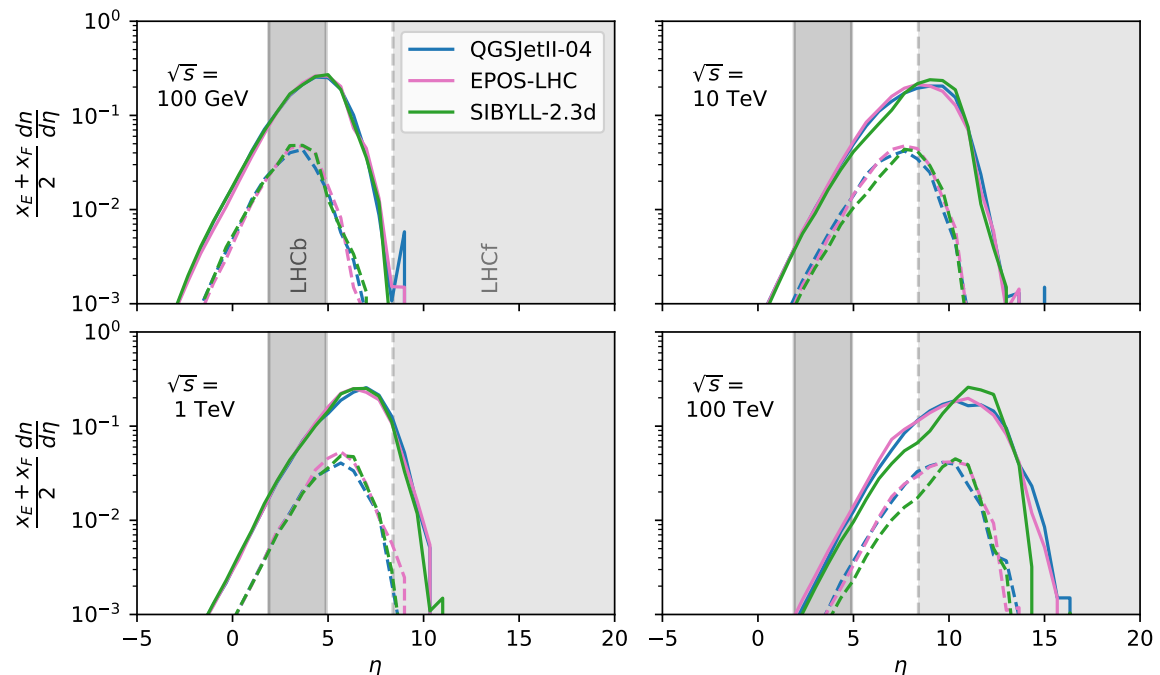


Figure 9. Weighted pseudorapidity distributions of all (solid lines) and EM-only (including π^0 , dashed lines) secondaries from proton-proton collisions at various center-of-mass energies for the three hadronic interaction models, computed with CRMC. The weight corresponds to the fraction of projectile energy carried by secondaries when boosted to the fixed-target rest frame, given by eq. (6.1). The pseudorapidity acceptance regions of LHCb ($1.9 < \eta < 4.9$ [7]) and LHCf ($|\eta| > 8.4$ [68]) are indicated in gray.

The part of the air shower evolution relevant to the muon number are the secondaries that carry away most of the projectile energy E_{proj} :

$$\frac{E'}{E_{\text{proj}}} \approx \frac{E + p_z}{\sqrt{s}} = \frac{x_E + x_F}{2}. \quad (6.1)$$

Here E and p_z are respectively the energy and (z -)momentum of the secondary. The prime denotes the Earth's rest frame, and the first equality follows from a boost to the center of mass frame (where $E' = \gamma(E + \beta p_z)$, with $\gamma = \sqrt{s}/(2m_p)$ and $\beta \approx 1$, and $E_{\text{proj}} \approx s/(2m_p)$). The second step follows from the definitions of $x_E \equiv 2E/\sqrt{s}$ and Feynman- x $x_F \equiv 2p_z/\sqrt{s}$. Since collider experiments detect secondaries in specific pseudorapidity intervals (and above energy thresholds), it is instructive to identify which pseudorapidity intervals contain most of the projectile energy. We show in figure 9 the pseudorapidity distributions computed with CRMC of all (solid lines) and only EM secondaries (dashed lines) from proton-proton interactions for various CM energies, weighted by eq. (6.1). There is a clear positive correlation between the CM energy and the pseudorapidity at which the distribution peaks, implying that different forward regions are relevant at different energies. An enhancement of r corresponds to reducing the area underneath the EM spectrum (dashed lines). In principle, pseudorapidity regions away from the peaks need not be affected, but this requires fine-tuning that may be

difficult to reconcile with an underlying physical model. Therefore, we consider the swapping of pions and kaons to be equivalently present in all kinematic regions. Note that since new physics would primarily arise in the constrained central regions, our approach could be regarded as conservative.

In the following we investigate the effect of swapping pions and kaons on the predictions of cosmic-ray hadronic interaction models in phase-space regions relevant for the LHCf and LHCb detectors. In particular, we assess whether current measurements permit an $O(40\%)$ of swapping as we found to be required for solving the muon puzzle (see the central plot in figure 8).

6.1 LHCf

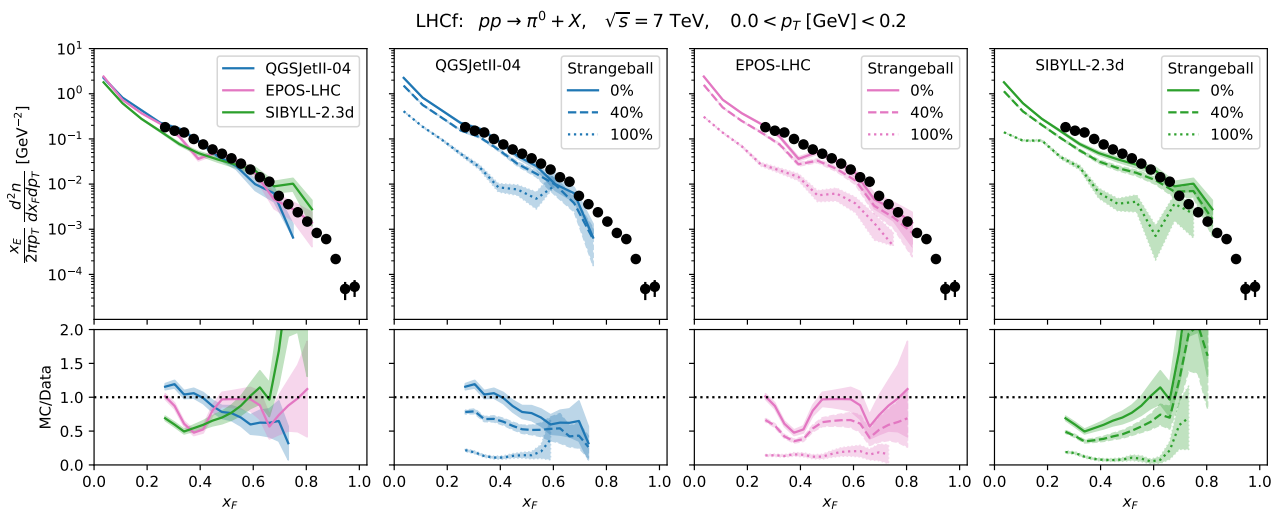


Figure 10. The neutral pion yield from proton-proton collisions at $\sqrt{s} = 7$ TeV as measured by the LHCf detector [68] (data points) and retrieved from various models with CRMC (lines), for the p_T -range of 0.0 to 0.2 GeV. For clarity, we separately visualize the effect of 40% and 100% strangeballs for each of the hadronic interaction models. The bands correspond to 1σ Monte Carlo uncertainties.

The LHCf measurements of the neutral pion yield from $\sqrt{s} = 7$ TeV proton-proton collisions [68] constrain the energy going into the EM component, i.e. the complement of r . A comparison of these measurements with model predictions is shown in figure 10, as well as the effect of a 40% and 100% strangeball (i.e., swapping pions and kaons). Note that here a 100% strangeball simply corresponds to the neutral kaon spectrum (both K_S^0 and K_L^0). At this energy the LHCf detector is only sensitive to the high-rapidity tail of the EM distribution (see figure 9), making only the $x_F < 0.4$ region relevant in practice for the muon number. While a 40% strangeball induces a significant suppression to the spectra, these deviations appear to be of the same order of magnitude as the model differences. Therefore, with the current theoretical uncertainties one cannot exclude a 40% strangeball on the basis of these data.

6.2 LHCb

The picture looks different when considering LHCb measurements of the K_S^0 p_T -spectrum produced by $\sqrt{s} = 900$ GeV proton-proton collisions [69], as shown in figure 11. Here, the

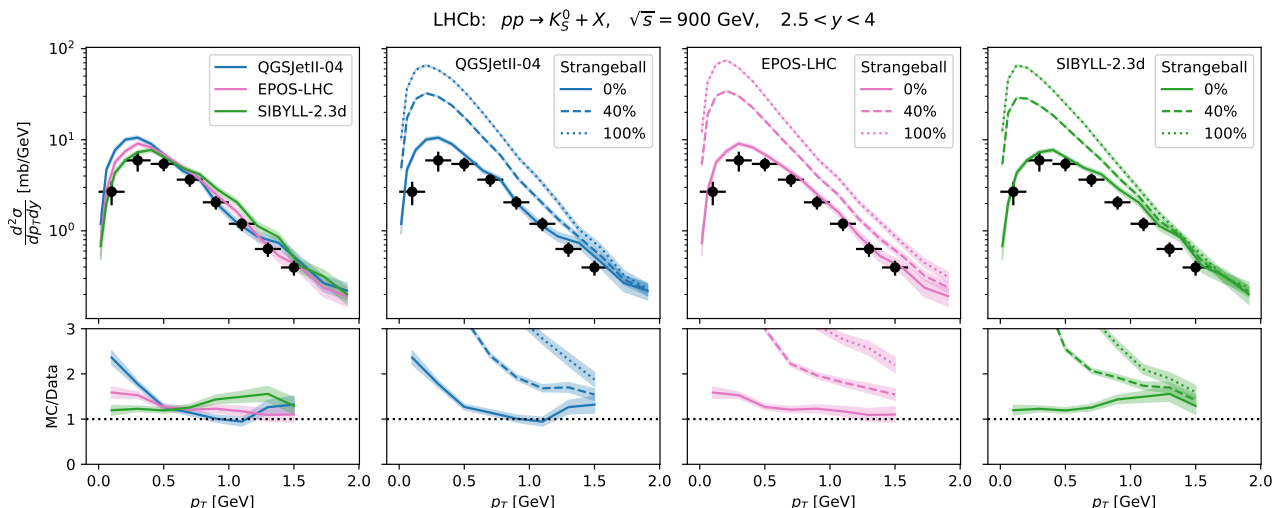


Figure 11. The K_S^0 p_T -spectrum from proton-proton collisions at $\sqrt{s} = 900$ GeV as measured by the LHCb detector [69] (data points) and retrieved from various models with CRMC (lines), for the rapidity range of 2.5 to 4. For clarity, we separately visualize the effect of 40% and 100% strangeballs for each of the hadronic interaction models. The bands correspond to 1σ Monte Carlo uncertainties.

introduction of 40% or 100% strangeballs significantly enhances the spectra as the more abundant neutral pions are converted to neutral kaons, breaking the reasonable agreement of the hadronic interaction models with the data. This seems to be a clear constraint on the strangeball model, especially given the relevant rapidity range for muon production (see figure 9). However, two caveats need to be considered in the interpretation of this data: the energy and the species of the colliding particles.

For proton-proton collisions this data implies that strangeballs may only appear at higher energies, requiring $E_{\min} > (900 \text{ GeV})^2 / (2m_p) = 4 \cdot 10^{14}$ eV. Looking at the left plot in figure 8 we then find solutions to the muon puzzle only at relatively low values for E_{\max} ($\lesssim 10^{18.5-19.5}$ eV), which competes with the constraint arising from muon fluctuations, requiring $E_{\max} \gtrsim 10^{19}$ eV. Exploiting this tension, the upcoming proton-proton LHC runs at $\sqrt{s} = 14$ TeV provides an opportunity to rule out the formation of strangeballs *from protons* as a solution to the muon puzzle. We suggest in particular the ratio of K_S^0 to the charged pion spectra as a clear indicator for strangeball-like effects, see figure 12.

It is important to emphasize that the previous discussion only concerns collisions between protons, and that the bulk of the interactions in air showers are those between pions and air (see, e.g., figure 1 of ref. [67]). Nuclear effects seem to be negligible as we found no difference in figure 12 when considering proton-oxygen collisions at 10 TeV. In contrast, having pions instead of protons as projectiles may play an important role. Unfortunately, it is experimentally challenging to produce charged pion beams for super-TeV center of mass collisions and look for strangeballs directly. Until then we depend on the synergy between indirect measurements at collider and air shower experiments, and the further development of hadronic interaction models to make progress.

Here we would like to add to this synergy by making a qualitative argument on the consequence of having pions as projectiles for the viability of the strangeball model. Since pions are more compact than protons, the same new physics (e.g., strangeballs) should be induced at lower energies. Inversely, the previously derived constraint on E_{\min} from $\sqrt{s} = 900$

GeV LHCb data is relaxed for pions. The hadronic cascade in air showers is fueled by interactions between projectile partons with relatively large x [66, 67] and thus target partons with small x . At small $x \equiv E_{\text{parton}}/E_{\text{hadron}}$, the parton distribution function (PDF) is dominated by gluons, falling as $x g(x, Q^2) \propto x^\alpha$ with $-0.29 \leq \alpha \leq -0.14$ at $x = 10^{-4}$ in various PDF sets [70]. Estimating the volume difference between pions and protons based on the number of valence quarks, the gluon volume density of pions is a factor $3/2$ that of protons. A proton-air interaction would achieve the same energy density at a factor $(3/2)^{1/\alpha} \approx 0.06 - 0.25$ in x , or $4 - 18$ in energy. This implies that for pion projectiles the constraint on E_{min} can be relaxed by about an order of magnitude, alleviating the tension with the muon fluctuations. Interestingly, this is not sufficient to avoid a constraint from measurements at $\sqrt{s} = 14 \text{ TeV} \Leftrightarrow E = 10^{17} \text{ eV}$. Therefore, the 40% strangeball deviation from the Standard Model shown in figure 12 is a concrete prediction of the strangeball model as a solution to the muon deficit.

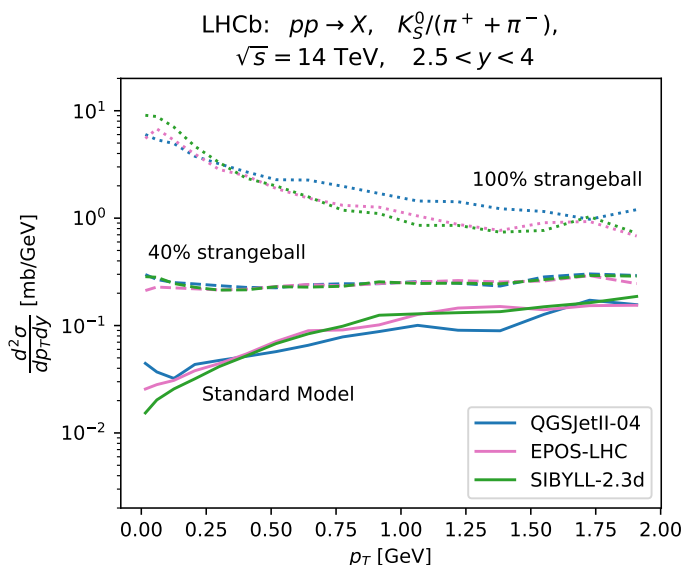


Figure 12. Ratio of K_S^0 to charged pion p_T -spectra from proton-proton collisions at $\sqrt{s} = 14 \text{ TeV}$, computed with CRMC, that could be measured by the LHCb detector to test the strangeball solution to the muon puzzle.

7 Conclusions

Adopting the phenomenological modeling of ref. [37], we exclude the production of fireballs in cosmic ray air showers as a resolution to the muon puzzle based on the fact that it introduces a tension between data on the average and fluctuations of X_{max} . This can be traced back to the fireball property of producing a plasma state, which enhances the inelasticity (and multiplicity) and thereby accelerates the shower development. Instead, we find the effect on X_{max} to be negligible when ignoring the formation of a plasma (modeled by repeated *in situ* collisions) and only considering enhancements to the strange quark content of the secondaries (modeled by swapping pions and kaons). This strangeness enhancement is found to be sufficient for resolving the muon puzzle at 10 EeV.

To make a clear distinction with the original fireball model, we denote the *strangeball* model as the model enhancing the strangeness without plasma formation. To test this strangeball model as a solution to the muon puzzle also at other energies, we extended the Heitler-Matthews model such that it can include variations in the fraction of energy remaining in the hadronic component. By fitting this to strangeball-extended CONEX simulations we inferred the parameters relevant for the strangeball model. With a subsequent application to Auger data we find a spectrum of solutions to the muon puzzle, characterized by two extremes: a sudden introduction of strangeballs at 10^{17} eV, making up the first few interactions, or a gradual introduction starting already at low energies ($< 10^{14}$ eV). Data on the relative muon fluctuations favors the latter extreme, implying that effects must be visible at energies accessible to collider experiments. At LHC and Tevatron energies, we find a solution to the muon puzzle to require 40% of the interactions to be strangeballs, corresponding to a sizable 5 – 9% increase of the energy retained in the hadronic cascade, with respect to predictions from current hadronic interaction models.

From a comparison with current LHC measurements we cannot directly exclude this scenario. The theoretical uncertainty on the model predictions for the neutral pion spectra as measured by the LHCf detector exceeds the effect from a 40% strangeball. While data from LHCb at $\sqrt{s} = 900$ GeV does exclude a strangeball, this constraint can be circumvented by only introducing strangeballs above 10^{14} eV. Note that this competes with the constraint from the muon fluctuations. This tension is relaxed by an order of magnitude when recognizing that air showers are dominated by pion-air interactions. We suggest a LHCb measurement of the ratio of p_T -spectra of K_S^0 to charged pions at $\sqrt{s} = 14$ TeV to be a powerful test for the strangeball scenario.

As final remarks we would like to emphasize that still much can be won on the astroparticle side of the muon puzzle. For example, including data from the underground muon detector of the Pierre Auger Observatory [71] — and in its extension also data from other experiments (see, e.g., ref. [6]) — in a similar analysis could further constrain the origin of the muon puzzle and provide more precise predictions for collider experiments. Along the same lines, also the reduction of the systematic and statistical uncertainties on respectively the average and relative fluctuations of the muon number will be beneficial. Finally, the concrete strangeball prediction of altering the strange particle content in air showers may affect more observables beyond the absolute muon number: the larger critical energy of kaons would give rise to a harder muon energy spectrum and a shallower muon production depth. The latter would actually improve the agreement with Auger data [72], motivating further studies in this direction as well.

It remains important to connect the particle and astroparticle physics communities as both are needed to solve the muon puzzle. The benefit to the astroparticle physics community is readily apparent, with precision determinations of the cosmic ray mass composition bringing us closer to revealing the cosmic ray origin. But the potential benefit to the particle physics community cannot be understated, considering the unique high-energy and ultra-high-energy laboratory provided by air showers. To sustainably drive this synergy we should work towards flexible (modular) and transparent hadronic interaction models. These would enable fundamental interpretations of astroparticle data in term of the underlying particle physics, as well as lay a solid foundation for studying the cosmos.

Acknowledgments

We thank Sergey Ostapchenko for lending us his expertise through critical comments and the ensuing discussions. We further thank Tanguy Pierog for his suggestions and help regarding the implementation of the fireball/strangeball model into CONEX. The simulations were performed on the PHYSnet Compute Cloud of the University of Hamburg. Luis Anchordoqui is acknowledged for useful communications. The work of M.V.G. was partially supported by the Bundesministerium für Bildung und Forschung, under contract 05H21GUCCA. J. M. and G.S. acknowledge support by the Bundesministerium für Bildung und Forschung, under grants 05A17GU1 and 05A20GU2.

References

- [1] THE PIERRE AUGER COLLABORATION, *Measurement of the cosmic-ray energy spectrum above 2.5×10^{18} eV using the Pierre Auger Observatory*, *Phys. Rev. D* **102** (2020) 062005.
- [2] THE PIERRE AUGER COLLABORATION, *Depth of maximum of air-shower profiles at the Pierre Auger Observatory. I. Measurements at energies above $10^{17.8}$ eV*, *Phys. Rev. D* **90** (2014) 122005.
- [3] THE PIERRE AUGER COLLABORATION, *Depth of maximum of air-shower profiles at the Pierre Auger Observatory. II. Composition implications*, *Phys. Rev. D* **90** (2014) 122006.
- [4] THE PIERRE AUGER COLLABORATION, *Evidence for a mixed mass composition at the ‘ankle’ in the cosmic-ray spectrum*, *Physics Letters B* **762** (2016) 288.
- [5] THE PIERRE AUGER COLLABORATION, *Inferences on mass composition and tests of hadronic interactions from 0.3 to 100 EeV using the water-Cherenkov detectors of the Pierre Auger Observatory*, *Phys. Rev. D* **96** (2017) 122003.
- [6] DEMBINSKI, H.P., ARTEAGA-VELÁZQUEZ, J.C., CAZON, L., CONCEIÇÃO, R., GONZALEZ, J., ITOW, Y. ET AL., *Report on Tests and Measurements of Hadronic Interaction Properties with Air Showers*, *EPJ Web Conf.* **210** (2019) 02004.
- [7] J. ALBRECHT ET AL., *The Muon Puzzle in cosmic-ray induced air showers and its connection to the Large Hadron Collider*, *Astrophys. Space Sci.* **367** (2022) 27 [2105.06148].
- [8] D. SOLDIN, *Update on the Combined Analysis of Muon Measurements from Nine Air Shower Experiments*, IN *Proceedings of 37th International Cosmic Ray Conference — PoS(ICRC2021)*, VOL. 395, P. 349, 2021, DOI: 10.22323/1.395.0349.
- [9] R. ULRICH, R. ENGEL AND M. UNGER, *Hadronic multiparticle production at ultrahigh energies and extensive air showers*, *Phys. Rev. D* **83** (2011) 054026.
- [10] S. BAUR, H. DEMBINSKI, M. PERLIN, T. PIEROG, R. ULRICH AND K. WERNER, *Core-corona effect in hadron collisions and muon production in air showers*, *arXiv e-prints* (2019) [1902.09265].
- [11] L.A. ANCHORDOQUI, C.G. CANAL, F. KLING, S.J. SCIUTTO AND J.F. SORIANO, *An explanation of the muon puzzle of ultrahigh-energy cosmic rays and the role of the Forward Physics Facility for model improvement*, *Journal of High Energy Astrophysics* (2022) .
- [12] J. MANSHANDEN, *Ultra-High-Energy Cosmic Rays: A Fireball Model to resolve the Deficit of Muons in Simulations of Extensive Air Showers*, PH.D. THESIS, UNIVERSITÄT HAMBURG, 2021. [HTTPS://EDISS.SUB.UNI-HAMBURG.DE/HANDLE/EDISS/9531](https://ediss.sub.uni-hamburg.de/handle/ediss/9531).
- [13] L.A. ANCHORDOQUI, H. GOLDBERG AND T.J. WEILER, *Strange fireball as an explanation of the muon excess in Auger data*, *Phys. Rev.* **D95** (2017) 063005 [1612.07328].

- [14] J. ALVAREZ-MUNIZ, L. CAZON, R. CONCEICAO, J.D. DE DEUS, C. PAJARES AND M. PIMENTA, *Muon production and string percolation effects in cosmic rays at the highest energies*, *arXiv e-prints* (2012) [[1209.6474](#)].
- [15] FARRAR, GLENNYS R. AND ALLEN, JEFFREY D., *A new physical phenomenon in ultra-high energy collisions*, *EPJ Web of Conferences* **53** (2013) 07007.
- [16] T. PIEROG, S. BAUR, H. DEMBINSKI, R. ULRICH AND K. WERNER, *Collective Hadronization and Air Showers: Can LHC Data Solve the Muon Puzzle ?*, IN *Proceedings of 36th International Cosmic Ray Conference — PoS(ICRC2019)*, VOL. 358, P. 387, 2019, DOI: [10.22323/1.358.0387](#).
- [17] T. PIEROG, S. BAUR, H. DEMBINSKI, M. PERLIN, R. ULRICH AND K. WERNER, *When heavy ions meet cosmic rays: potential impact of QGP formation on the muon puzzle*, IN *Proceedings of 37th International Cosmic Ray Conference — PoS(ICRC2021)*, VOL. 395, P. 469, 2021, DOI: [10.22323/1.395.0469](#).
- [18] THE PIERRE AUGER COLLABORATION, *The Pierre Auger Cosmic Ray Observatory*, *Nucl. Instrum. Methods Phys. Res. A* **798** (2015) 172.
- [19] J.F. CARLSON AND J.R. OPPENHEIMER, *On Multiplicative Showers*, *Phys. Rev.* **51** (1937) 220.
- [20] W. HEITLER, *The Quantum Theory of Radiation*, OXFORD UNIVERSITY PRESS (1954).
- [21] J. MATTHEWS, *A Heitler model of extensive air showers*, *Astroparticle Physics* **22** (2005) 387.
- [22] A. ANDRONIC, P. BRAUN-MUNZINGER AND J. STACHEL, *Thermal hadron production in relativistic nuclear collisions: The Hadron mass spectrum, the horn, and the QCD phase transition*, *Phys. Lett. B* **673** (2009) 142 [[0812.1186](#)].
- [23] P. BRAUN-MUNZINGER, V. KOCH, T. SCHÄFER AND J. STACHEL, *Properties of hot and dense matter from relativistic heavy ion collisions*, *Phys. Rept.* **621** (2016) 76 [[1510.00442](#)].
- [24] K. DUSLING, W. LI AND B. SCHENKE, *Novel collective phenomena in high-energy proton–proton and proton–nucleus collisions*, *Int. J. Mod. Phys. E* **25** (2016) 1630002 [[1509.07939](#)].
- [25] P. KOCH, B. MÜLLER AND J. RAFELSKI, *From Strangeness Enhancement to Quark–Gluon Plasma Discovery*, *Int. J. Mod. Phys. A* **32** (2017) 1730024 [[1708.08115](#)].
- [26] W. BUSZA, K. RAJAGOPAL AND W. VAN DER SCHEE, *Heavy Ion Collisions: The Big Picture, and the Big Questions*, *Ann. Rev. Nucl. Part. Sci.* **68** (2018) 339 [[1802.04801](#)].
- [27] M. GAZDZICKI, M. GORENSTEIN AND P. SEYBOTH, *Brief history of the search for critical structures in heavy-ion collisions*, *Acta Phys. Polon. B* **51** (2020) 1033 [[2004.02255](#)].
- [28] ALICE, *The ALICE experiment – A journey through QCD*, [2211.04384](#).
- [29] BRAHMS, *Quark gluon plasma and color glass condensate at RHIC? The Perspective from the BRAHMS experiment*, *Nucl. Phys. A* **757** (2005) 1 [[NUCL-EX/0410020](#)].
- [30] PHENIX, *Formation of dense partonic matter in relativistic nucleus-nucleus collisions at RHIC: Experimental evaluation by the PHENIX collaboration*, *Nucl. Phys. A* **757** (2005) 184 [[NUCL-EX/0410003](#)].
- [31] STAR, *Experimental and theoretical challenges in the search for the quark gluon plasma: The STAR Collaboration’s critical assessment of the evidence from RHIC collisions*, *Nucl. Phys. A* **757** (2005) 102 [[NUCL-EX/0501009](#)].
- [32] F. BECATTINI AND J. MANNINEN, *Strangeness production from SPS to LHC*, *J. Phys. G* **35** (2008) 104013 [[0805.0098](#)].
- [33] ALICE, *Multiplicity Dependence of Pion, Kaon, Proton and Lambda Production in p-Pb Collisions at $\sqrt{s_{NN}} = 5.02$ TeV*, *Phys. Lett. B* **728** (2014) 25 [[1307.6796](#)].

- [34] ALICE, *Multi-strange baryon production in p-Pb collisions at $\sqrt{s_{\text{NN}}} = 5.02$ TeV*, *Phys. Lett. B* **758** (2016) 389 [[1512.07227](#)].
- [35] ALICE, *Enhanced production of multi-strange hadrons in high-multiplicity proton-proton collisions*, *Nature Phys.* **13** (2017) 535 [[1606.07424](#)].
- [36] D. LAHURD AND C.E. COVAULT, *Exploring Potential Signatures of QGP in UHECR Ground Profiles*, *JCAP* **11** (2018) 007 [[1707.01563](#)].
- [37] J.F. SORIANO, L.A. ANCHORDOQUI, T.C. PAUL AND T.J. WEILER, *Probing QCD approach to thermal equilibrium with ultrahigh energy cosmic rays*, *PoS ICRC2017* (2018) 342 [[1811.07728](#)].
- [38] P. BOZEK, *Size of the thermal source in relativistic heavy-ion collisions*, *Acta Phys. Polon. B* **36** (2005) 3071 [[NUCL-TH/0506037](#)].
- [39] K. WERNER, *Core-corona separation in ultra-relativistic heavy ion collisions*, *Phys. Rev. Lett.* **98** (2007) 152301 [[0704.1270](#)].
- [40] J. AICHELIN AND K. WERNER, *Centrality Dependence of Strangeness Enhancement in Ultrarelativistic Heavy Ion Collisions: A Core-Corona Effect*, *Phys. Rev. C* **79** (2009) 064907 [[0810.4465](#)].
- [41] F. BECATTINI AND J. MANNINEN, *Centrality dependence of strangeness production in heavy-ion collisions as a geometrical effect of core-corona superposition*, *Phys. Lett. B* **673** (2009) 19 [[0811.3766](#)].
- [42] M.M. BLOCK, L. DURAND, P. HA AND F. HALZEN, *Comprehensive fits to high energy data for σ , ρ , and B and the asymptotic black-disk limit*, *Phys. Rev. D* **92** (2015) 114021 [[1511.02406](#)].
- [43] T. PIEROG ET AL., *First results of fast one-dimensional hybrid simulation of EAS using CONEX*, *Nucl. Phys. B Proc. Suppl.* **151** (2006) 159 [[ASTRO-PH/0411260](#)].
- [44] T. BERGMANN, R. ENGEL, D. HECK, N.N. KALMYKOV, S. OSTAPCHENKO, T. PIEROG ET AL., *One-dimensional Hybrid Approach to Extensive Air Shower Simulation*, *Astropart. Phys.* **26** (2007) 420 [[ASTRO-PH/0606564](#)].
- [45] T. PIEROG, R. ENGEL AND D. HECK, *3D Air Shower Simulations Using CONEX in CORSIKA*, IN *Proc. 31 st Int. Cosmic Ray Conf., Lodz (Poland), (2009) contr. 0425*, [HTTP://ICRC2009.UNI.LODZ.PL/PROC/PDF/ICRC0425.PDF](http://icrc2009.uni.lodz.pl/proc/pdf/icrc0425.pdf).
- [46] T. PIEROG, R. ENGEL, D. HECK AND R. ULRICH, *3D hybrid air shower simulation in CORSIKA*, IN *32nd Internat. Cosmic Ray Conf., Beijing, China, August 11-18, 2011. Vol. 2*, PP. 222–225, 2012, DOI: [10.7529/ICRC2011/V02/1170](#).
- [47] D. HECK, J. KNAPP, J. CAPDEVIELLE, G. SCHATZ AND T. THOUW, *CORSIKA: A Monte Carlo Code to Simulate Extensive Air Showers*, *Forschungszentrum Karlsruhe Report FZKA* **6019** (1998) .
- [48] THE PIERRE AUGER COLLABORATION, *Muons in Air Showers at the Pierre Auger Observatory: Mean Number in Highly Inclined Events*, *Phys. Rev. D* **91** (2015) 032003 [[1408.1421](#)].
- [49] THE PIERRE AUGER COLLABORATION, *The Pierre Auger Observatory: Contributions to the 36th International Cosmic Ray Conference (ICRC 2019)*, *arXiv e-prints* (2019) [[1909.09073](#)].
- [50] S. OSTAPCHENKO, *Monte Carlo treatment of hadronic interactions in enhanced Pomeron scheme: QGSJET-II model*, *Phys. Rev. D* **83** (2011) 014018.
- [51] S. OSTAPCHENKO, *QGSJET-II: physics, recent improvements, and results for air showers*, *EPJ Web Conf.* **52** (2013) 02001.

- [52] T. PIEROG, I. KARPENKO, J.M. KATZY, E. YATSENKO AND K. WERNER, *EPOS LHC: Test of collective hadronization with data measured at the CERN Large Hadron Collider*, *Phys. Rev. C* **92** (2015) 034906.
- [53] F. RIEHN, R. ENGEL, A. FEDYNITCH, T.K. GAISSER AND T. STANEV, *Hadronic interaction model sibyll 2.3d and extensive air showers*, *Phys. Rev. D* **102** (2020) 063002.
- [54] S. BASS, M. BELKACEM, M. BLEICHER, M. BRANDSTETTER, L. BRAVINA, C. ERNST ET AL., *Microscopic models for ultrarelativistic heavy ion collisions*, *Progress in Particle and Nuclear Physics* **41** (1998) 255.
- [55] M. BLEICHER, E. ZABRODIN, C. SPIELES, S.A. BASS, C. ERNST, S. SOFF ET AL., *Relativistic hadron-hadron collisions in the ultra-relativistic quantum molecular dynamics model*, *J. Phys. G: Nucl. Part. Phys.* **25** (1999) 1859.
- [56] S. FUKUI, H. HASEGAWA, T. MATANO, I. MIURA, M. ODA, K. SUGA ET AL., *A Study on the Structure of the Extensive Air Shower*, *Progress of Theoretical Physics Supplement* **16** (1960) 1.
- [57] L. CAZON, R. CONCEIÇÃO AND F. RIEHN, *Probing the energy spectrum of hadrons in proton air interactions at ultrahigh energies through the fluctuations of the muon content of extensive air showers*, *Physics Letters B* **784** (2018) 68.
- [58] T. BIRO, H. NIELSEN AND J. KNOLL, *Colour rope model for extreme relativistic heavy ion collisions*, *Nuclear Physics B* **245** (1984) 449.
- [59] C. BIERLICH, G. GUSTAFSON, L. LÖNNBLAD AND A. TARASOV, *Effects of Overlapping Strings in pp Collisions*, *JHEP* **03** (2015) 148 [[1412.6259](#)].
- [60] C. BIERLICH, S. CHAKRABORTY, G. GUSTAFSON AND L. LÖNNBLAD, *Jet modifications from colour rope formation in dense systems of non-parallel strings*, *SciPost Phys.* **13** (2022) 023 [[2202.12783](#)].
- [61] C. BIERLICH, S. CHAKRABORTY, G. GUSTAFSON AND L. LÖNNBLAD, *Strangeness enhancement across collision systems without a plasma*, *Phys. Lett. B* **835** (2022) 137571 [[2205.11170](#)].
- [62] R. ULRICH, T. PIEROG AND C. BAUS, *Cosmic Ray Monte Carlo Package, CRMC*, AUG., 2021. DOI: [10.5281/ZENODO.5270381](#).
- [63] A. FEDYNITCH, F. RIEHN, R. ENGEL, T.K. GAISSER AND T. STANEV, *Hadronic interaction model sibyll 2.3c and inclusive lepton fluxes*, *Phys. Rev. D* **100** (2019) 103018.
- [64] S. GRIMM, D. VEBERIC AND R. ENGEL, *Heitler-Matthews model with leading-particle effect*, *PoS ICRC2017* (2017) 299.
- [65] THE PIERRE AUGER COLLABORATION, *Measurement of the Fluctuations in the Number of Muons in Extensive Air Showers with the Pierre Auger Observatory*, *Phys. Rev. Lett.* **126** (2021) 152002.
- [66] A. HILLAS, *Shower simulation: lessons from MOCCA*, *Nuclear Physics B - Proceedings Supplements* **52** (1997) 29.
- [67] M. REININGHAUS, R. ULRICH AND T. PIEROG, *Air shower genealogy for muon production*, *PoS ICRC2021* (2021) 463 [[2108.03266](#)].
- [68] LHCf COLLABORATION, *Measurements of longitudinal and transverse momentum distributions for neutral pions in the forward-rapidity region with the LHCf detector*, *Phys. Rev. D* **94** (2016) 032007.
- [69] LHCb COLLABORATION, *Prompt K_s^0 production in pp collisions at $\sqrt{s} = 0.9$ TeV*, *Phys. Lett. B* **693** (2010) 69 [[1008.3105](#)].

- [70] R.D. BALL, E.R. NOCERA AND J. ROJO, *The asymptotic behaviour of parton distributions at small and large x* , *Eur. Phys. J. C* **76** (2016) 383 [1604.00024].
- [71] THE PIERRE AUGER COLLABORATION, *Direct measurement of the muonic content of extensive air showers between 2×10^{17} and 2×10^{18} eV at the Pierre Auger Observatory*, *Eur. Phys. J. C* **80** (2020) 751.
- [72] THE PIERRE AUGER COLLABORATION, *Muons in air showers at the Pierre Auger Observatory: Measurement of atmospheric production depth*, *Phys. Rev. D* **90** (2014) 012012.

A Relative Muon Fluctuations

The relative shower-to-shower fluctuation of the muon number $\sigma(N_\mu)/\langle N_\mu \rangle$ is mainly determined by the physics of the first interaction [56, 57]: fluctuations from subsequent interactions average out. The Pierre Auger Collaboration measured the size of these fluctuations above 4 EeV [65], constraining the production of strangeballs above this energy. We consider the measurements presented at the ICRC in 2019 [49].

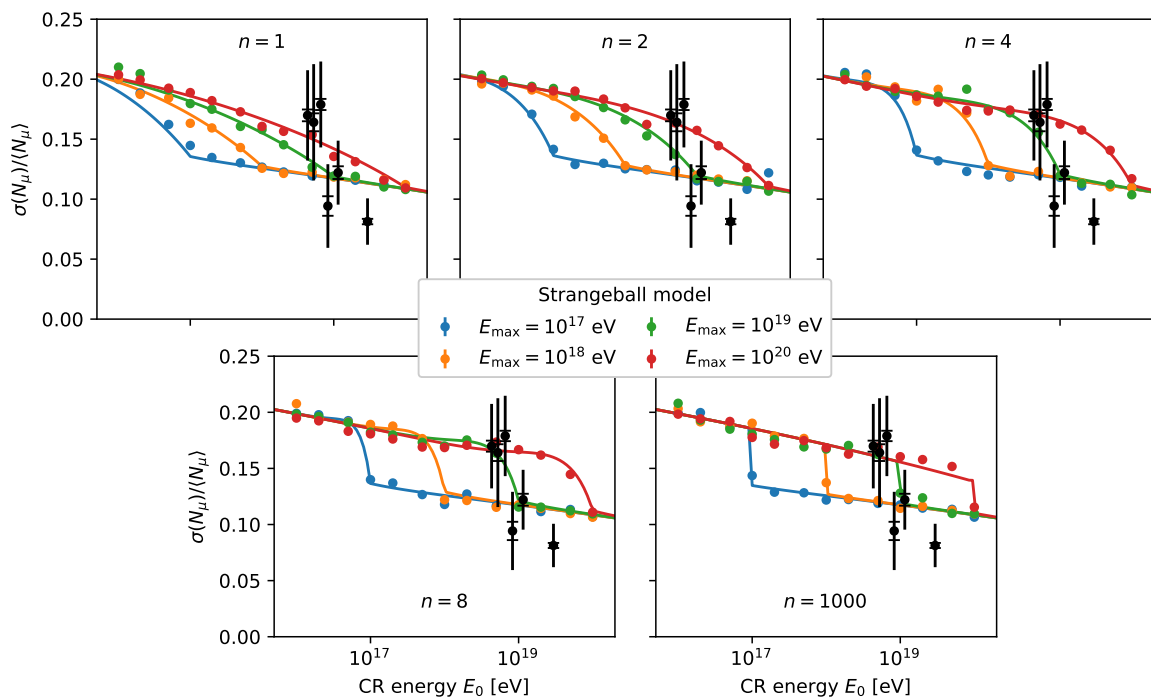


Figure 13. Energy dependence of the relative muon fluctuations from strangeball-extended CONEX simulations with EPOS-LHC (colored points) for various strangeball settings: $E_{\min} = 10^{15}$ eV is fixed, while E_{\max} (colors) and n (plots) vary. These simulations are fitted with our model (colored lines, eq. (A.7)), whose fit parameters are summarized in table 3. The black data points are from the Pierre Auger Observatory as presented at the ICRC in 2019 [49].

From our strangeball-extended CONEX simulations we find that introducing the strangeball model reduces the relative muon fluctuations. This is visualized with proton primaries in figure 13: above E_{\max} the fluctuations reach a slightly declining plateau between 0.15 and 0.10. For $n = 1000$ and $E_0 < E_{\max}$ one retrieves the Standard Model result, which corresponds to a similar plateau that is approximately 0.05 higher. The transition between the

plateaus is determined by the strangeball settings through the strangeball probability $p(E)$ of eq. (2.2). A suppression of the relative muon fluctuations may be a general feature of any model that increases the hadronic energy fraction. We will get back to this at the end of the appendix.

We exclude the strangeball settings for which the predictions for proton CR primaries fall more than 1σ (combined systematic and statistical uncertainties) below the data points from the Pierre Auger Observatory. Note that these constraints are actually more stringent since the X_{\max} -inferred composition requires the data to be below the proton prediction (see, e.g., figure 2 of ref. [65]). The constraints turn out to be mostly on E_{\max} , with that from the first (third) data point excluding the region to the left of the dashed (double-dot dashed) lines in figure 7.

To derive these constraints we constructed a model describing the energy dependence of the relative muon fluctuations, as described below.

A.1 Modeling Relative Muon Fluctuations

We follow a similar approach as in section 4, starting from the principles of the Heitler-Matthews model.

With the critical energy fixing the total number of particles N_{tot} and a generational picture of air showers, the muon number N_{μ} can be decomposed into a product of hadronic energy fractions r_i at generation i from the first generation until the critical generation k_c :

$$N_{\mu} = N_{\text{tot}} \prod_{i=1}^{k_c} r_i . \quad (\text{A.1})$$

Fluctuations then arise from variations of these hadronic energy fractions and from variations of the total number of generations. For our modeling, we fix the total number of generations to k_c , effectively ignoring shower-to-shower fluctuations of the multiplicity. This is expected to be a subdominant effect since the value of β (see eq. (4.1)) is close to 1 when inferred from Standard Model simulations. See ref. [57] and in particular the discussion around eq. (4) of this reference for more details.

A generational picture of air showers implies that the hadronic energy fraction at each generation is independent of the next. Therefore, the variance of the muon number can be decomposed as

$$\text{var}(N_{\mu}) = \text{var} \left(N_{\text{tot}} \prod_{i=1}^{k_c} r_i \right) = N_{\text{tot}}^2 \prod_{i=1}^{k_c} [\sigma^2(r_i) + \langle r_i \rangle^2] - N_{\text{tot}}^2 \prod_{i=1}^{k_c} \langle r_i \rangle^2 , \quad (\text{A.2})$$

where $\sigma^2(r_i)$ and $\langle r_i \rangle$ are the variance and average of the hadronic energy fraction at generation i , respectively. The relative muon fluctuations can then be written as

$$\frac{\sigma(N_{\mu})}{\langle N_{\mu} \rangle} = \sqrt{\prod_{i=1}^{k_c} \left[1 + \left(\frac{\sigma(r_i)}{\langle r_i \rangle} \right)^2 \right]} - 1 . \quad (\text{A.3})$$

Here r_i is the hadronic energy fraction of an entire generation and its fluctuations are suppressed by the number of particles N_i in that generation: $\sigma(r_i) = \sigma(r_{\text{eff}})/\sqrt{N_i}$. This explicitly shows the dominance of the first interaction.

The effective hadronic energy fraction of an interaction r_{eff} is given by a superposition of strangeball and Standard Model interactions (eq. (4.2)), which can be propagated to the (squared) relative fluctuations as

$$\frac{\sigma^2(r_{\text{eff}})}{\langle r_{\text{eff}} \rangle^2} = \frac{(1-p)\sigma^2(r_{\text{SM}}) + p\sigma^2(r_{\text{sb}})}{[(1-p)\langle r_{\text{SM}} \rangle + p\langle r_{\text{sb}} \rangle]^2} + \frac{p(1-p)[\langle r_{\text{sb}} \rangle - \langle r_{\text{SM}} \rangle]^2}{[(1-p)\langle r_{\text{SM}} \rangle + p\langle r_{\text{sb}} \rangle]^2}, \quad (\text{A.4})$$

where we suppressed the energy dependence of $p \equiv p(E)$ for readability.

From a comparison with CONEX simulations it turns out that a continuous extension of the product in eq. (A.3) provides a better description (see ref. [12] for more details):

$$\prod_{i=1}^{k_c} \left[1 + \left(\frac{\sigma(r_i)}{\langle r_i \rangle} \right)^2 \right] \rightarrow \exp \left\{ \int_0^{k_c} \log \left[1 + \left(\frac{\sigma(r_i)}{\langle r_i \rangle} \right)^2 \right] dk + \Delta_{\text{corr}} \right\}. \quad (\text{A.5})$$

Similar to eq. (4.3) we have a correction factor,

$$\Delta_{\text{corr}} = \frac{1}{2} \log \left[1 + \left(\frac{\sigma(r_i)}{\langle r_i \rangle} \Big|_{k=0} \right)^2 \right], \quad (\text{A.6})$$

corresponding to half a generation of the integrand, with the ratio of moments evaluated at the first interaction. Physically, this continuous representation allows us to include particles with energies ‘between’ the generations and thereby partly take into account the elasticity of interactions in real air showers.

We nevertheless stick to a generational picture with synchronized shower branches and the energy equally divided over all secondaries. As in section 4, this allows us to use the multiplicity to relate the generation k to the energy E of the secondaries, and the total number of particles is simply $N = E_0/E$.

Putting everything together we have

$$\frac{\sigma(N_\mu)}{\langle N_\mu \rangle} = \sqrt{\exp \left[\int_{\log E_0}^{\log E_c} \log \left(1 + \frac{\sigma^2(r_{\text{eff}}) E}{\langle r_{\text{eff}} \rangle^2 E_0} \right) \frac{dk}{d \log E} d \log E + \frac{1}{2} \log \left(1 + \frac{\sigma^2(r_{\text{eff}})}{\langle r_{\text{eff}} \rangle^2} \Big|_{E=E_0} \right) \right] - 1}, \quad (\text{A.7})$$

with $\sigma^2(r_{\text{eff}})/\langle r_{\text{eff}} \rangle^2$ given in eq. (A.4) and the Jacobian for a power-law multiplicity (eq. (4.4)) given by

$$\frac{dk}{d \log E} = \frac{1}{\log(1-b)} \frac{1}{\log(n_{\text{scale}}^{1/b} E/\text{GeV})}. \quad (\text{A.8})$$

These two terms significantly complicate the energy dependence of the integrand, preventing an analytic evaluation of the integral. Considering eq. (A.4), not only the strangeball probability $p(E)$ (eq. (2.2)), but also $\langle r_{\text{SM}} \rangle$, $\langle r_{\text{sb}} \rangle$, $\sigma(r_{\text{SM}})$, and $\sigma(r_{\text{sb}})$ may be energy dependent. It turns out that the declining plateau features in figure 13 cannot be reproduced without this additional energy dependence, and thus we parametrize the variances as $\sigma^2(x) = \alpha - \beta \log_{10}(E/\text{GeV})$, with $x \in \{r_{\text{SM}}, r_{\text{sb}}\}$.

With this we obtain a good fit to the CONEX simulations as shown in figure 13 for EPOS-LHC. Similarly good fits are obtained for QGSJETII-04 and SIBYLL-2.3D, with all

parameters summarized in table 3. Note that these parameters differ from those listed in table 2, indicating that our picture is still a simplification of real air showers. We also found a good agreement with CONEX simulations at $E_{\min} = 10^{14}$ eV and 10^{16} eV, justifying the interpolation in also this strangeball setting.

We end with a comment on the suppression of the relative muon fluctuations. At energies sufficiently above E_{\max} , the first part of the shower consists of strangeballs and thus $\sigma(N_\mu)/\langle N_\mu \rangle$ is an accumulation of $\sigma(r_{\text{sb}})/\langle r_{\text{sb}} \rangle$ from the first few interactions. The same holds for the Standard Model at energies below E_{\min} (or below E_{\max} with high n). The energy dependencies of $\sigma(r_{\text{sb}})/\langle r_{\text{sb}} \rangle$ and $\sigma(r_{\text{SM}})/\langle r_{\text{SM}} \rangle$ thus form the declining plateau features, whose heights are determined by the sizes of these relative fluctuations. Since the hadronic energy fraction is bound from above by 1 (which limits the fluctuations), and from CRMC simulations we have $0.5 < \langle r_{\text{SM}} \rangle < \langle r_{\text{sb}} \rangle$ (table 2), we can expect $\sigma(r_{\text{sb}})/\langle r_{\text{sb}} \rangle < \sigma(r_{\text{SM}})/\langle r_{\text{SM}} \rangle$. This propagates to a plateau with a lower height for the strangeball model. The same argument holds for any model that increases the average hadronic energy fraction, with the exception of fine-tuned scenarios invoking a simultaneous, disproportional increase of the probability of events with low hadronic energy fractions.

Table 3. Fit parameters for modeling the relative muon fluctuations of strangeball-extended CONEX simulations with eq. (A.7). The variances of the hadronic energy fractions are parametrized as $\sigma^2 = \alpha - \beta \log_{10}(E/\text{GeV})$.

	$\langle r_{\text{SM}} \rangle$	$\langle r_{\text{sb}} \rangle$	$\sigma^2(r_{\text{SM}})$		$\sigma^2(r_{\text{sb}})$		b	n_{scale}
			α	β	α	β		
QGSJetII-04	0.669	0.840	0.100	0.00196	0.0743	0.00140	0.00184	51.29
EPOS-LHC	0.504	0.643	0.0621	0.00114	0.0428	0.000719	0.190	2722
Sibyll-2.3d	0.531	0.658	0.0663	0.00117	0.0527	0.000897	0.177	2429